

## Paleoseismic transect across the northern Great Basin

Steven G. Wesnousky,<sup>1</sup> Andrew D. Barron,<sup>1</sup> Richard W. Briggs,<sup>1</sup> S. John Caskey,<sup>2</sup> Senthil Kumar,<sup>1</sup> and Lewis Owen<sup>3</sup>

Received 30 June 2004; revised 22 January 2005; accepted 11 February 2005; published 25 May 2005.

[1] The relationship of strain accumulation to strain release over different timescales provides insight to the dynamics, structural development, and spatial and temporal pattern of earthquake recurrence in regions of active tectonics. The Great Basin physiographic province of the western United States is one of the Earth's broadest regions of ongoing continental extension, encompassing an area reaching  $\sim 800$  km in width between the Sierra Nevada to the west and Wasatch mountains to the east. We present observations arising from excavations, scarp profiling, optically stimulated luminescence, and radiocarbon dating to place limits on the late Pleistocene paleoseismic history of faults bounding eight ranges across the interior of the northern Great Basin, specifically, the Shawave, Hot Springs, Humboldt, Sonoma, Shoshone, Tuscarora, Dry Hills, and Pequop ranges. Combining the observations with similar previously published studies within and at the margins of the Great Basin yields a transect that extends eastward across the basin between the 40th and 41st parallels. The sum of observations provides a picture of the patterns and rates of earthquake recurrence over the region during the last  $\sim 20$ – $45$  kyr that may be compared to patterns of contemporary seismicity and recently reported measures of strain accumulation across the area using GPS. The recurrence rate of large surface rupture paleoearthquakes along ranges at the margins of the Great Basin is systematically greater than observed along ranges in the interior. The pattern is similar to seismological and geodetic measurements that show levels of background seismicity and strain accumulation are also concentrated along the margins of the Great Basin. An east-west extension rate across the interior of the Great Basin on the order of  $1/2$  mm yr<sup>-1</sup> (strain rate of  $\sim 1$  nstrain yr<sup>-1</sup>) over the last  $\sim 20$ – $45$  kyr is estimated by summing the record of paleoseismic displacements across the 400 km breadth of the transect, as compared to  $\sim 2$  mm yr<sup>-1</sup> of strain accumulation indicated by a recently reported analysis of a collinear GPS survey. The comparison is hindered by significant uncertainties coupled to the geologic rate estimate. The transect also crosses the northern limit of the central Nevada seismic belt. The central Nevada seismic belt is defined by a north-northeast trending alignment of historical surface rupture earthquakes, increased levels of background seismicity, and strain accumulation rates greater than observed elsewhere in the interior of the Great Basin. The reported recurrence rate of late Pleistocene surface rupture earthquakes within the central Nevada seismic belt is also generally greater than observed along our transect. The observations when taken together suggest that the characteristics of strain release observed historically within the central Nevada seismic belt have been operative over the latest Pleistocene and that the apparently greater rates of strain accumulation and release in the central Nevada seismic belt are diminished or less localized in regions to the north and east. Thus, while the historical alignment of surface ruptures that defines the central Nevada seismic belt remains a unique clustering of earthquakes in time and space, the likelihood of the cluster at its observed location appears greater than would be expected to the north or eastward in the interior of the Great Basin.

**Citation:** Wesnousky, S. G., A. D. Barron, R. W. Briggs, S. J. Caskey, S. Kumar, and L. Owen (2005), Paleoseismic transect across the northern Great Basin, *J. Geophys. Res.*, *110*, B05408, doi:10.1029/2004JB003283.

<sup>1</sup>Center for Neotectonic Studies, University of Nevada, Reno, Nevada, USA.

<sup>2</sup>Department of Geosciences, San Francisco State University, San Francisco, California, USA.

<sup>3</sup>Department of Earth Sciences, University of California, Riverside, California, USA.

## 1. Introduction

[2] The Great Basin physiographic province of the western United States is characterized by Basin and Range style deformation and encompasses an area reaching  $\sim 800$  km in width between the stable Sierra Nevada block to the west and the Wasatch mountains to the east (Figure 1). The deformation has been attributed to a combination of buoyancy forces and accommodation of right-lateral transform motion across the Pacific-North America plate boundary subsequent to the Miocene inception of the San Andreas fault system [Bennett *et al.*, 2003; Jones *et al.*, 1996; Sonder and Jones, 1999; Thatcher *et al.*, 1999]. Relative right-lateral Pacific-North America plate motion of  $\sim 50$  mm yr<sup>-1</sup> averaged over the last  $\sim 3$  Myr [DeMets and Dixon, 1999] is virtually the same as measured with space geodesy [e.g., Sella *et al.*, 2002]. Plate motion models [e.g., Minster and Jordan, 1984], geologic observations [e.g., Dokka and Travis, 1990; Reheis and Dixon, 1996], and geodesy [Bennett *et al.*, 1998; Dixon *et al.*, 1995; Oldow *et al.*, 1994; Reheis and Dixon, 1996; Sauber, 1994; Sauber *et al.*, 1986; Savage *et al.*, 1995; Thatcher *et al.*, 1999] indicate that 15% to 25% of the  $\sim 50$  mm yr<sup>-1</sup> of relative right-lateral motion is distributed to the east of the Sierra Nevada and across the Great Basin.

[3] The accommodation of relative plate motion and buoyancy forces internal to the crust and mantle have resulted in 120 to 150 km or greater of extension of the Great Basin during the last  $\sim 10$  to 20 my [Sonder and Jones, 1999]. The relatively uniform spacing of about two dozen mountain ranges and the similarity in elevation differences between adjacent mountains and valleys have been cited to suggest that the cumulative long-term deformation is distributed relatively uniformly across the region [Bennett *et al.*, 1998; Wallace, 1984b]. In contrast, the distribution and style of seismicity and faulting is not uniform across the Great Basin. Seismicity is concentrated at the eastern and western boundaries within the Intermountain seismic belt and Walker Lane, respectively, and within the central Nevada seismic belt (Figure 1) where large surface rupture earthquakes during the last  $\sim 130$  years define a coherent, northeast trending, sequential, alignment of activity (Figure 2). The surface rupture earthquakes were separated by only a few months to a few decades and the basis for Wallace [1984a] to define the alignment as the central Nevada seismic belt. As well, active faulting in the Walker Lane is dominated by northwest striking right-lateral faults while faulting to the east is primarily normal on northeast striking faults.

[4] Space-based geodetic measurements reveal a pattern of strain accumulation that largely reflects the spatial distribution of faulting and historical seismicity. The Intermountain seismic belt occurs along a zone of concentrated strain equivalent to about  $\sim 3$  mm yr<sup>-1</sup> of westerly extension (Figures 1 and 2) [Bennett *et al.*, 2003]. Modern strain rates are sufficiently small between the Intermountain and central Nevada seismic belts to lead Bennett *et al.* [2003] to approximate the region as a rigid block. The highest rates of strain are localized on the western side of the basin, within an area encompassing the central Nevada seismic belt and Walker Lane, where measurements indicate the equivalent of  $\sim 10$  mm yr<sup>-1</sup> of right-lateral shear oriented parallel to

the Walker Lane [Bennett *et al.*, 2003; Thatcher *et al.*, 1999]. South of  $\sim 38.5^\circ\text{N}$ , the strain is taken up primarily by strike-slip faults in the Walker Lane. To the north, the strain is distributed between strike-slip faulting in the Walker Lane and predominantly normal faulting eastward to the central Nevada seismic belt. There is currently uncertainty concerning whether or not the level of increased strain rate associated with the central Nevada seismic belt is a long-lived feature of the strain field. For example, the relatively greater strain within the central Nevada seismic belt may in part reflect a transient postseismic viscoelastic response from the historical earthquakes [Hetland and Hager, 2003]. Likewise, it is not clear if the level of increased strain rate continues northward beyond the belt of historical earthquakes that define the Central Nevada Seismic Belt (Figures 1 and 2). The east trending geodetic transect of the USGS (Figure 1) [Hammond and Thatcher, 2004; Thatcher, 2003; Thatcher *et al.*, 1999] shows a sharp increase in velocity across the central Nevada seismic belt, whereas a similarly rapid increase is not clear in the like oriented though spatially less dense BARGEN network of Bennett *et al.* [1998, 2003] to the north (Figure 1).

[5] Toward examining whether or not the pattern of modern strain accumulation and release is evident in the late Pleistocene record of fault displacements, we present observations bearing on the timing of late Pleistocene earthquake displacements on eight fault-bounded range fronts across the northern Great Basin: the Shawave, Hot Springs, Humboldt, Sonoma, Shoshone, Tuscarora, Dry Hills, and Pequop ranges (Figure 2). The observations are then combined with prior studies of the same type to provide an initial illustration of the pattern of strain release by large earthquakes across the northern Great Basin during late Pleistocene.

## 2. Methods

[6] We employ the now standard approach of excavating trenches across the scarps of active faults preserved in late Pleistocene alluvium [e.g., McCalpin, 1996]. Trenches in this study are preferably sited along pronounced fault scarps that bound the major mountain fronts, cut late Pleistocene and younger surfaces, and show morphological expression of repeated late Pleistocene offsets. The details of site locations are provided in the following observations section. Exposed stratigraphic and structural relationships are the basis for estimates of the timing and normal displacement component of earthquakes that produced the scarps. Radiocarbon dating of organic materials and correlation of tephra deposits are used when available to place limits on the age of geologic units exposed in the trenches and hence the age of past earthquake displacements. The results, methodology, and laboratories used for radiocarbon analysis are summarized in Table 1. The identification of tephra is provided by the Tephrochronology Laboratory at the U.S. Geological Survey (USGS) in Menlo Park that is overseen by A. M. Sarna-Wojcicki following the approach described by Sarna-Wojcicki and Davis [1991]. At one locality, ages of stratigraphic units are reported from analysis of optically stimulated luminescence (OSL) provided by the Luminescence Dating Laboratory at University

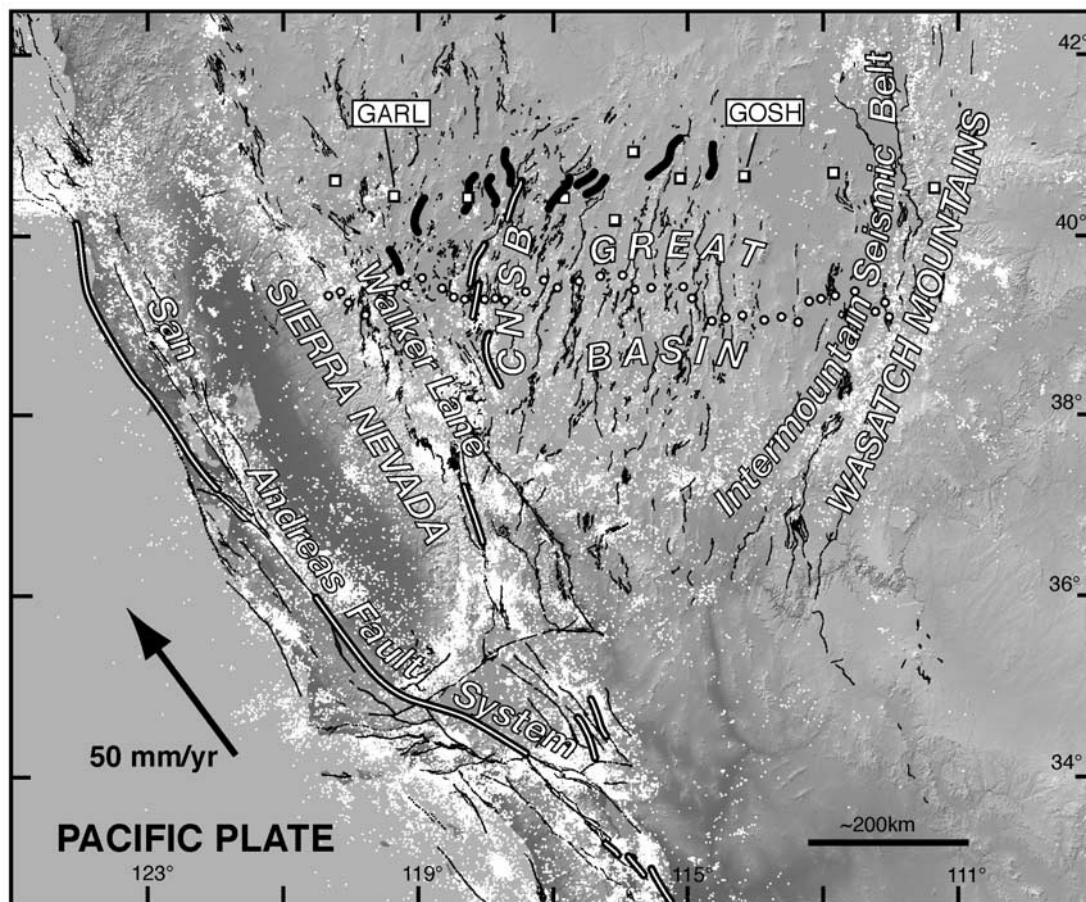


**Figure 1.** Active faults (thin and thick solid lines) and seismicity (dots,  $M > 2$  since 1944) plotted on shaded relief map of Great Basin province and surrounding areas. Thick solid lines denote faults subject to paleoseismological study by authors. Thick open lines are extent of historical earthquake ruptures [Goter *et al.*, 1992]. CNSB is central Nevada seismic belt. Locations of GPS stations surveyed by USGS are shown by open circles south of  $40^{\circ}\text{N}$  [Hammond and Thatcher, 2004; Thatcher, 2003; Thatcher *et al.*, 1999]. Selected GPS station locations of BARGEN array north of  $40^{\circ}\text{N}$  marked by open squares [Bennett *et al.*, 1998, 2003]. Stations GARL and GOSH labeled in reference to discussion in text. Fault map is adapted from parts of Jennings [1994], Dohernwend *et al.* [1996], and the Fault and Fold Database of the U.S. Geological Survey [Haller *et al.*, 2004; <http://qfaults.cr.usgs.gov>]. Seismicity is from the Advanced National Seismic System's composite catalog (<http://quake.geo.berkeley.edu/anss/catalog-search.html>). Plate motion vector is from DeMets and Dixon [1999]. See color version of this figure at back of this issue.

of California Riverside using the collection and mineral preparation techniques outlined by Richards [2000] and Owen *et al.* [2001] and measurement procedures described by Owen *et al.* [2003].

[7] The degree of soil development is also locally used to gauge the relative age of Quaternary alluvial surfaces displaced by the active faults. Soil nomenclature follows Birkeland [1999]. We limit attention primarily to the thickness, structure, and relative clay content and carbonate development of B-horizons, all of which have been observed to increase as a function of time [e.g., Birkeland, 1999; Harden, 1982; Machette, 1978].

[8] In instances where scarps are the result of a single earthquake and exposures yielded no dateable material, estimates of the age of the scarp-forming event are derived from the morphology of the scarp. The topographic expression of a fault scarp degrades in a systematic manner as a

function of time and initial scarp height [Bucknam and Anderson, 1979; Wallace, 1977]. Hanks and Wallace [1985] represent the process of scarp degradation using the diffusion equation which, expressed in the homogeneous form with constant coefficients, is written  $du/dt - \kappa(d^2u/dx^2) = 0$ , where  $u(x, t)$  is the elevation of a point on the scarp at time  $t$ ,  $x$  is the horizontal (cross-fault strike) distance, and  $\kappa$  is a constant of proportionality with the units of diffusivity in  $\text{m}^2 \text{kyr}^{-1}$ . The solution to the equation for the case where far-field slopes of the footwall and hanging wall surfaces are not zero is delivered in detail by Hanks and Andrews [1989]. The solution provides the capability to formulate synthetic scarp profiles for specific values of the product of diffusivity and time ( $\kappa t$ ) that may be compared directly to measured scarp profiles. The solution is a function of the slopes of the foot (beta<sub>up</sub>) and hanging wall (beta<sub>low</sub>) surfaces, the vertical separation across the scarp

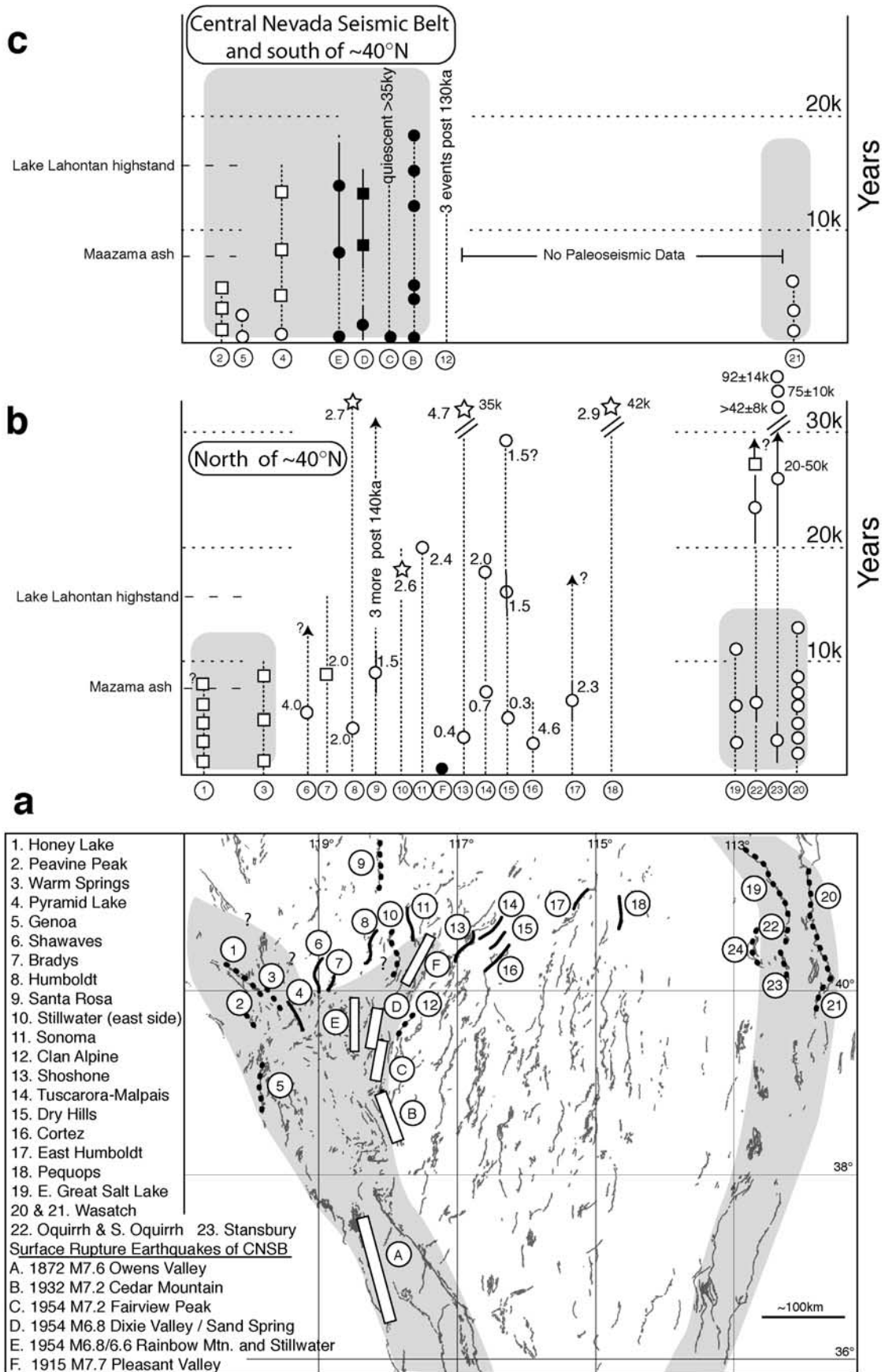


Figure 2

**Table 1.** Radiocarbon Samples

Location	Sample Lab ID <sup>a</sup>	<sup>14</sup> C Age <sup>b</sup> ±2σ	δ <sup>13</sup> C, ‰ <sup>c</sup>	Calendar Age <sup>d</sup> ±2σ, years B.P.	Calendar Age <sup>d</sup> ±2σ, years B.C.	Material
Shawaves	SHA1-01-SGW	2040 ± 40	-20	1898–2115	166 B.C. to 52 A.D.	bird bone
	CAMS-79167			<b>2007 ± 108</b>		
Shawaves	SHA3-05-SGW	4720 ± 40	-24.3	5323–5584	3,635–3,374	soil
	GX-30533			<b>5453 ± 109</b>		
Humboldts	SGW-HUMT1-02	4085 ± 30	-25	4445–4808	2,859–2,496	charcoal
	CAMS-80362			<b>4626 ± 181</b>		
Sonomas	SGW-ST1-1	16960 ± 110	-23.1	19533–20881	18,932–17,584	soil
	GX-30363			<b>20027 ± 674</b>		
Shoshones	LCT-RC1-SGW	6030 ± 40	-25	6748–6986	5,037–4,799	charcoal
	CAMS-71529			<b>6867 ± 119</b>		
Shoshones	LCT3-RC1	2950 ± 50	-20.9	2953–3317	1,368–1,004	soil
	GX-30364			<b>3317 ± 364</b>		
Tuscarora-Malpais	BEO1-03-SGW	6550 ± 40	-21.5	7338–7563	5,614–5,389	soil
	GX-29214-AMS			<b>7450 ± 112</b>		
Tuscarora-Malpais	BEO1-05-SGW	15640 ± 60	-21.3	18119–19283	17,334–16,170	soil
	GX-29215-AMS			<b>18701 ± 582</b>		
Dry Hills	DHT-Bulk1	5065 ± 35	-25	5734–5907	3,958–3,785	burnt seed
	CAMS-90556			<b>5820 ± 87</b>		

<sup>a</sup>Samples processed at Center for Accelerator Mass Spectrometry (CAMS) at Lawrence Livermore National Laboratory and Geochron Laboratories (GX) in Cambridge, Massachusetts. Top of two labels at each location are field sample numbers.

<sup>b</sup>Uses Libby's half-life 5568 years.

<sup>c</sup>The δ<sup>13</sup>C values are the assumed values according to *Stuiver and Polach* [1977, p. 355] when given without decimal places. Values measured for the material itself are given with a single decimal place.

<sup>d</sup>Dendrochronologically calibrated ages calculated with Web-based University of Washington calibration program (CALIB 4.4) [*Stuiver and Reimer*, 1993; *Stuiver et al.*, 1998]. Values given according to convention as bracketing ages and as median value with plus/minus uncertainties (bold) for convenience of discussion in text.

(offset),  $\kappa t$ , and an assumed value of friction ( $\mu$ ) that defines the initial angle of repose for a scarp in weakly consolidated fan materials [*Hanks and Andrews*, 1989]. In this manner, we use the linear diffusion model of *Hanks and Andrews* [1989], and set friction at 0.75 while the remaining variables are adjusted to produce a synthetic scarp profile that visually best matches the observed scarp profile. Independent estimates of scarp diffusivity  $\kappa$  are then used to place bounds on the age of the most recent surface rupture earthquake. For this, we draw upon the collection of diffusivity estimates put forth and reviewed by *Hanks* [2000] that suggest  $\kappa$  values of  $\sim 1 \text{ m}^2 \text{ kyr}^{-1}$  for late Pleistocene fault and wave-cut scarps in unconsolidated alluvium in the Great Basin, and estimates of  $\kappa$  arising from analysis of independently dated fault scarps in this study. The uncertainties attendant to the determination of  $\kappa$  values are detailed by *Hanks* [2000].

[9] The scarp profiles analyzed in this study are gathered for later discussion in Figure 3. For each locality, the observed profile is compared to the best fitting synthetic profile, and a visual measure of the closeness of fit is provided by plotting the RMS misfit between observed and synthetic profile versus a broad range of  $\kappa t$ , while holding all other variables constant and equal to the values that yield the best fitting synthetic.

### 3. Observations

[10] The observations that provide the basis for interpretation are presented here. The reader may be better served by first reading the Discussion and Conclusion section. There, the sum of observations and the hypotheses arising from those observations are synthesized and discussed with Figure 2 and, in turn, provide a useful context to then

**Figure 2.** (a) Active fault map of Great Basin province. Faults studied by the authors are highlighted by solid bold lines, and those reported previously by others are depicted by bold dashed lines. Major surface rupture earthquakes that delineate the central Nevada seismic belt (Figure 1) are enclosed by boxes. Number or letter adjacent to each box corresponds to fault and name of surface rupture earthquakes, respectively, given at left and listed in Table 2. Earthquake magnitudes are from *Goter et al.* [1994]. Shading approximates areas of relatively increased crustal strain rate within Great Basin adapted from GPS studies of *Thatcher et al.* [1999] and *Bennett et al.* [2003]. Space versus time history of earthquake surface ruptures during late Pleistocene on faults located (b) north and (c) south of approximately 40°N. Vertical axes are time and horizontal axes distance, and horizontal axes are scaled approximately to map in Figure 2a. Fault corresponding to each rupture sequence is labeled with fault number along horizontal axis. Circles are individual earthquake surface rupture times constrained by history or stratigraphy, with error bars provided when reported greater than symbol dimension. Squares approximately placed to indicate constraint indicating a certain number of events after a particular age horizon. Stars are ages estimated by analysis of fault scarp profiles and given for convenience of presentation without error bars, which are likely on the order of 10 kyr. Solid symbols are used for faults in the central Nevada seismic belt. Lack of earthquakes at times older than the extent of vertical dashed lines reflects a lack of observational data for each earthquake sequence. Spatial extent of time histories of faults in regions of elevated geodetic strain and the central Nevada seismic belt are also shaded in Figures 2b and 2c.

review the necessarily detailed documentation of observations pertaining to each fault.

### 3.1. Shawave and Blue Wing Mountains

[11] The Shawave and Blue Wing Mountains are west tilted fault blocks and bounded by Granite Springs Valley on the east (Figure 4). The east flanks of the mountains are bounded by a ~40-km-long east dipping normal fault. Vertical relief across the fault approaches a kilometer, with ridgelines of the Shawaves commonly exceeding 2100 m and the flats of Granite Springs Valley situated at about 1200 m. The Shawave Mountains are primarily granodiorite and the Blue Wing Mountains metasedimentary rocks of Cretaceous and Jurassic age [Johnson, 1977]. The fault is expressed locally by an abrupt and faceted range front, the truncation of fan and pediment surfaces and as relatively continuous scarps in young alluvium along the entire fault length. Trenches were excavated across the fault at sites along the Shawave and Blue Wing mountain ranges (Figure 4).

[12] The abrupt truncation of older fan and pediment surfaces marks the trace of the fault in the vicinity of the Shawave Trench (Figure 5). The trench site is located where the fault cuts a ~1.5-m-high scarp that cuts young alluvium debouching from the mouth of an unnamed canyon. The trench log is shown in Figure 6a. The trench exposure consists entirely of granitic coarse sand and pebble gravel with a minor percentage of small cobbles. Beds of alluvial sand and gravel (unit 1) dip subhorizontally, are the oldest units in the exposure, and are broken by two near vertical fault strands. The displacement of unit 1 across the fault strands appears to be ~1.5 m, but is uncertain due to the similarity in the characteristics of the beds comprising unit 1. Beds of unit 2 in the hanging wall are alluvial cut and fill deposits that have eroded into and sit upon unit 1. Units 1 and 2 and the two fault strands are capped by scarp derived colluvium (unit 3) consisting of poorly sorted coarse and granular sand lacking any layered fabric. Unit 4 is composed of medium beds of poorly sorted coarse sand with a few percent of small cobbles and interpreted to be alluvium derived from the adjacent small drainage. An 8-mm-long, cylindrical and hollow bone of 1–2 mm diameter was collected from the base of unit 4 (sample SHA1-01-SGW) and determined to be  $2007 \pm 108$  cal years B.P. old (Table 1). The scarp-derived

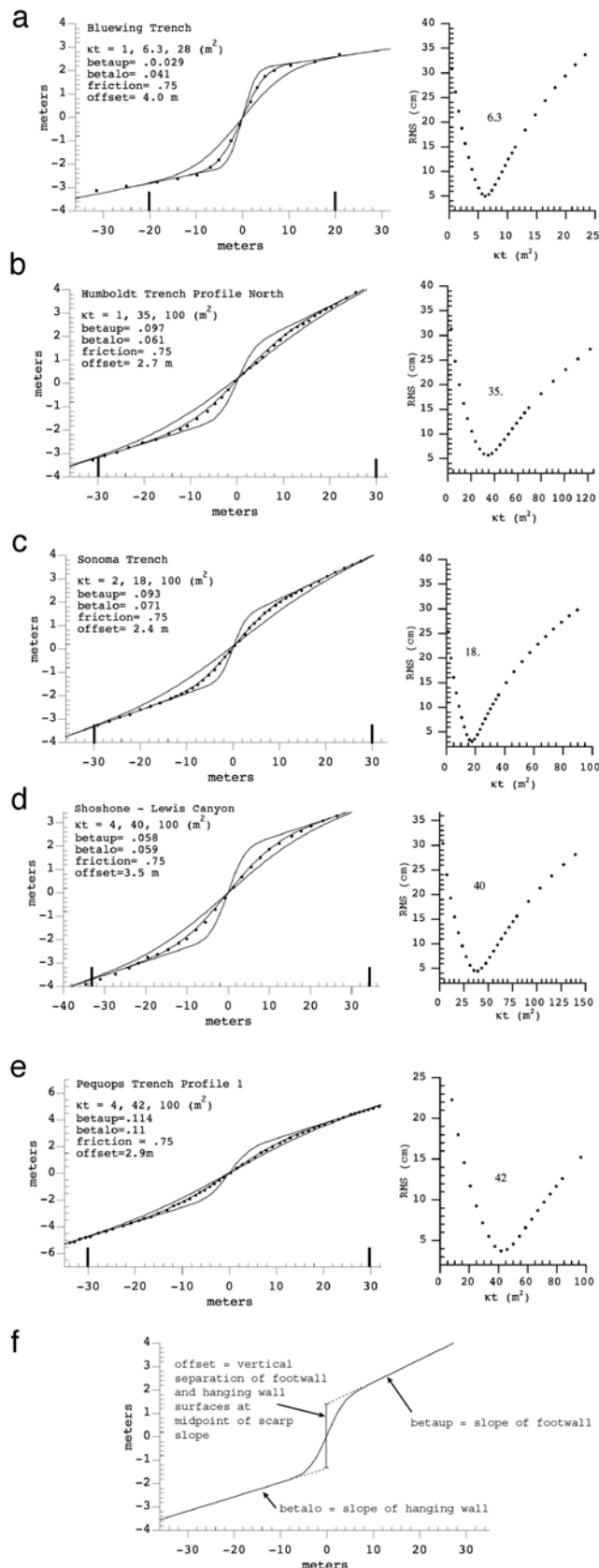


**Figure 3.** Analysis of fault scarps using diffusion equation at (a) Bluewing, (b) Humboldt, (c) Sonoma, (d) Shoshone-Lewis Canyon, and (e) Pequop trench sites. (left) Measured (dots) and synthetic profiles (lines) of scarp adjacent to trenches computed for values of  $\kappa_T$  listed. Values of  $\kappa_T$  are those that yield the best fit of the synthetic to the observed profile and two bounding values of  $\kappa_T$ . Listed are the assumed value of friction, the offset (vertical separation of offset surfaces), and the values of footwall (betaup) and hanging wall (betalo) slopes used to compute the synthetic profiles. Vertical bars along horizontal axis mark extent over which root mean square misfits are calculated. (right) Root mean square misfits of synthetic to observed profiles as a function of  $\kappa_T$ . The value of  $\kappa_T$  resulting in the minimum misfit is listed. (f) Values of offset, betaup, and betalo.

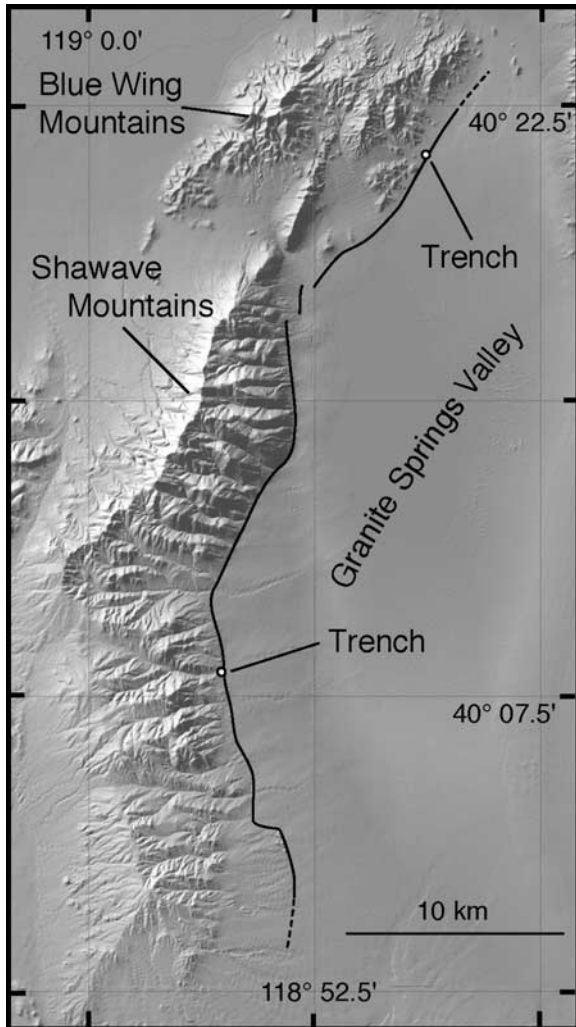


**Figure 4.** Trench site locations on the active normal fault (solid line) that bounds the east flank of the Shawave and Blue Wing mountains. Fault is labeled 6 in Figure 2.

colluvium (unit 3) and depositional beds of unit 4 are not cut by the fault strands and therefore postdate the most recent displacement. The radiocarbon age of the bone (sample SHA1-01-SGW, Table 1) indicates the most recent displacement occurred prior to  $2007 \pm 108$  cal years B.P.

[13] The northern trench site is located along the Blue Wing Mountains where the trace cuts a broad alluvial fan complex (Figures 4 and 7). The  $\sim 50$  m trench exposes a fault graben. A massive matrix supported angular platy cobble-boulder debris flow (unit 1) is the oldest unit exposed in the trench (Figure 6b). Units 2 and 3 are alluvial fan gravels that consist of poorly sorted, subangular, discontinuous, subhorizontal lenses and beds of cobble and boulder gravel reaching  $\sim 0.5$  m thickness. Unit 3 is distinguished from unit 2 by a lighter tone and an increased fine sand and silt component. Units 4 and 5 are distinct beds of poorly sorted coarse sand and cobble alluvial fan. Units 3 and 4 extend across the entire exposure. Units 1–5 are all faulted. Unit 6 is scarp derived colluvium. The entire exposure with the exception of the steeper portions of the scarp is capped by a  $\sim 5$ - to 10-cm-thick silt cap (Av soil horizon).

[14] Discontinuous 1- to 3-cm-thick lenses of volcanic ash occur between units 4 and 5 on both the footwall and hanging wall of the western scarp (Figure 6b). An ash located nearby in a similar stratigraphy beneath the faulted surface is chemically similar to the Maazama ash, from which we infer the scarp forming event occurred after  $7627 \pm 150$  cal years B.P. [Zdanowicz *et al.*, 1999]. Analogous to the present-day Av horizon, the Av horizon that existed on the surface at the time of the last fault displacement is well preserved as a  $\sim 5$ -cm-thick layer beneath the scarp-derived colluvium (unit 6). The radiocarbon age of the organic fraction of the buried Av horizon is  $5453 \pm 109$  cal years B.P. (sample SHA3-05-SGW, Table 1). The organic fraction of the soil horizon reflects a process whereby younger carbon is continuously added to the soil while older carbon is lost by processes of decay and translocation and, hence, the radiocarbon age of the buried Av horizon may be somewhat older than the time of burial [Anderson *et al.*, 2002; Birkeland, 1999].

[15] The vertical separation of the ground surface across the western scarp at the Blue Wing mountain trench is  $\sim 4$  m (Figure 3a, 6b, and 7) and virtually the same as the vertical offset of the base of unit 3. The observation, in conjunction with the presence of only a single package of scarp-derived colluvium, indicates that the scarp is due to a single event and that a scarp did not exist here prior to the most recent event. The same is true on the eastern back facing scarp where vertical separation is about 0.75 m. Reconstruction of the section to take into account the 4 m displacement on the main western fault juxtaposes units 1 and 2, and that mismatch of units is evidence of prior recurrent Quaternary displacement. Although the observation provides no quantitative constraint on the age of a penultimate earthquake, one may infer a long period of erosion was required prior to the recent displacement to completely remove any preexisting scarp here and elsewhere along strike where the trace cuts young alluvium.

[16] The similarity of the morphologic expression of the fault scarp at and in between the Shawave and Blue Wing trench sites suggests the entire range front fault ruptured simultaneously during the last earthquake. The trench

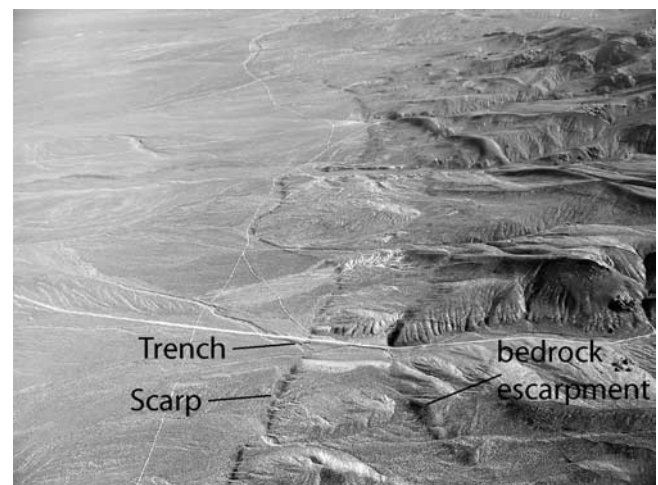


**Figure 5.** Fault scarp and trench site along Shawave Mountains. View to the south.

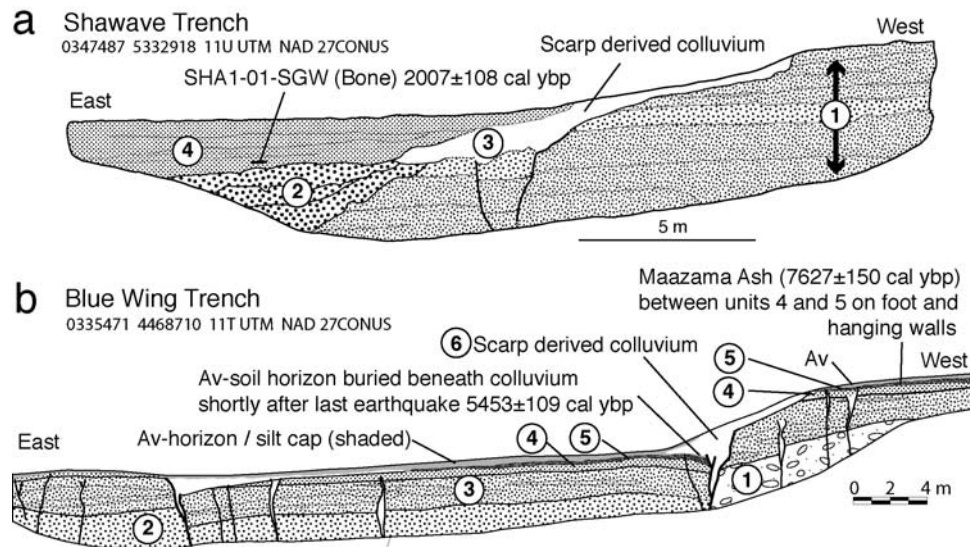


**Figure 6.** Sketch of exposures in trenches along the (a) Shawave and (b) Blue Wing mountains. Unit label numbers correspond to description in text. Locations are described by UTM coordinates and in Figures 4, 5, and 7.

exposures and reconnaissance along the fault trace suggest vertical displacements during the last surface rupture event commonly reached values on the order of 3 m. When combining the dates of both trenches, the event occurred between  $2007 \pm 108$  and  $7627 \pm 150$  cal years B.P., and most likely closest in time to  $5453 \pm 109$  cal years B.P.

[17] A profile of the scarp surveyed adjacent to the trench and synthetic profiles constructed using the diffusion equation are shown in Figure 3a. The best fit of a synthetic curve to the observed is found for vertical separation of 4 m and  $\kappa t = 6.3 \text{ m}^2$ . Dividing the value of  $\kappa t = 6.3 \text{ m}^2$  by the best estimate of the scarp age ( $\sim 5500$  years) yields an estimate of the scarp diffusivity  $\kappa = 1.2$ , in general accord with prior estimates of  $\kappa$  in the region [Hanks, 2000].

### 3.2. Hot Springs Mountains: Bradys Fault

[18] The Hot Springs Mountains reach an elevation of 1634 m at Desert Peak,  $\sim 400$  m above the adjacent basin (Figure 8). The northern portion of the range is a faulted and north trending anticline composed of diatomaceous sediments and volcanics ranging from Pliocene to Miocene in age [Axelrod, 1956]. The Bradys fault strikes northeastward and subparallel to the west flank of the mountains (Figure 8). The southwestern end of the scarp is defined by an alignment of fumaroles. We excavated the fault where it produces an  $\sim 2$ -m-high scarp in alluvium. The trench log is shown in Figure 9. Unit 1 is interbedded fine and coarse sand, with some coarser beds composed entirely of reworked diatomite. Unit 2 is a planar-bedded fine sand with occasional cross beds and thins and pinches out away from the fault zone. Unit 3 is clast supported, subrounded to rounded pebble and cobble gravel of lacustrine origin that forms distinct east dipping foresets. The lacustrine foresets of unit 3 likely formed during the recession of pluvial Lake Lahontan. Lake Lahontan reached its highstand  $\sim 13,000$   $^{14}\text{C}$  year BP ( $\sim 15,500$  cal years B.P. [e.g., Adams and Wesnousky, 1998]). Units 1, 2, and 3 are offset

vertically about 2 m across a west dipping normal fault. Unit 4 is a mix of colluvium derived from the scarp degradation and aeolian input. The unit is generally massive, very fine sand and silt supporting a minor component of subangular to rounded clasts. The similarity in the amount of displacement ( $\sim 2$  m) of all beds in the section shows the surface scarp is due to a single event. Hence, the exposure indicates only one surface rupture earthquake subsequent to the highstand of Lake Lahontan. Additionally, the match of facies and bed thicknesses across the fault trace is consistent with pure normal displacement. The large aeolian input to unit 4 indicates the shape of the scarp is not solely due to processes of mass diffusion and amenable to scarp diffusion analysis.

### 3.3. Humboldt Range

[19] The peaks of the Humboldt Range rise to elevations of  $\sim 2900$  m above the adjacent basins at  $\sim 1300$  m



**Figure 7.** Fault scarp and trench site along Blue Wing Mountains. View is to southwest.

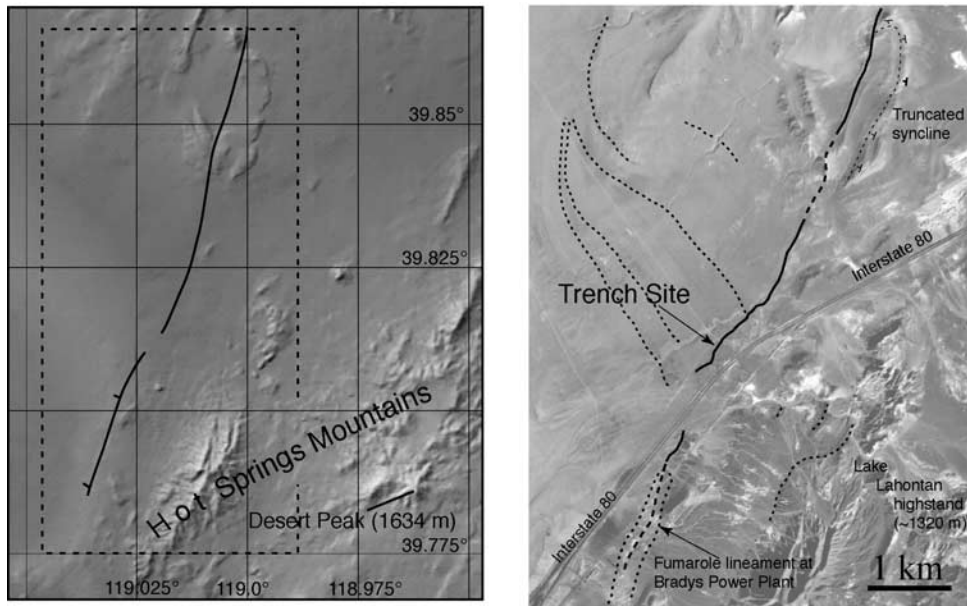


**Figure 8.** (left) Bradys fault trace (bold line, ticks on hanging wall) on shaded relief map. (right) Fault trace (bold) and trench site annotated on air photo (trace dashed where approximate). Dashed lines near trench site are trend of prominent lacustrine shoreline features of pluvial Lake Lahontan. Extent of photo is outlined by dashed box at left. Fault is labeled 7 in Figure 2.

(Figure 10). The range is a horst and composed primarily of Permo-Triassic metasedimentary and intrusive rocks [Silberling and Wallace, 1967; Wallace et al., 1969]. The Quaternary expression of faulting is greatest along the western flank. Youthful and repeated movement along the range front fault is expressed by offset of deposits of pluvial Lake Lahontan and the truncation and progressively greater uplift of older alluvial fan deposits (Figure 11).

[20] The log of a trench excavated across a strand of the fault at the site depicted in Figure 11b is offered in Figure 12. The footwall east of the fault (unit 1) is medium and thick beds of poorly sorted, subangular pebble, cobble, and small boulder alluvial gravel, with both clast and matrix supported layers. The upper ~1 m of unit 1 is overprinted by pedogenic carbonate that reaches stage 3 [Birkeland, 1999] development. The beds of unit 2 on the hanging wall are similar to unit 1, though individual beds within each unit are not clearly correlated across the fault. The lack of correlation may be real or obfuscated by soil development and erosion of the footwall surface. Sitting on unit 2 is a wedge-shaped package of gravel interpreted to be scarp-

derived colluvium (unit 3). The colluvium displays a west dipping fabric and is composed of massive poorly sorted sand with a minor component of pebbles and cobbles that decreases westward away from the fault. The colluvium is permeated and well cemented by stage 2–3 pedogenic carbonate. At the western end of the trench where unit 3 thins, the horizon of pedogenic carbonate overprints unit 2 and displays similar carbonate development approaching that observed on footwall unit 1. The scarp-derived colluvium is broken by two fault strands. The fault strands bound a fissure (unit 4). The fissure is filled by poorly sorted subangular pebble and cobble gravel at the base that grades upward into massive, fine sand and silt. Charcoal derived from woody plants is disseminated throughout the fissure at depths of 1–2.5 m. Radiocarbon analysis of a sample places the age of the charcoal at  $4626 \pm 181$  cal years B.P. (sample SGW-HUMT1-02, Table 1).

[21] The Humboldt trench exposure records the occurrence of two or more surface rupture earthquakes. The most recent occurred near in time to  $4626 \pm 181$  cal years B.P.,

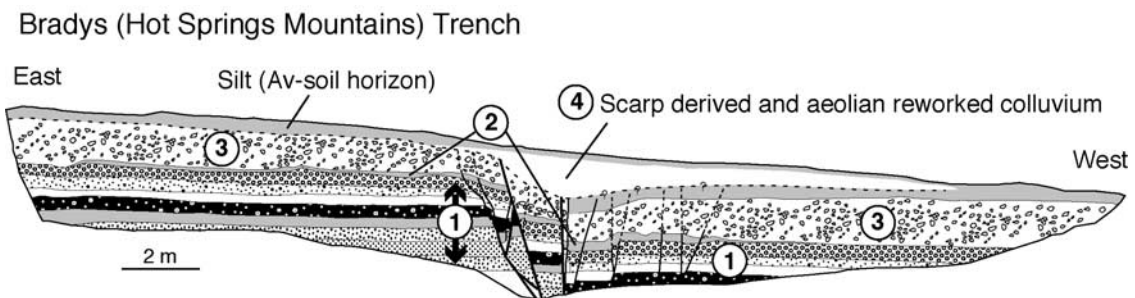


**Figure 9.** Sketch of trench exposure across Bradys fault. Unit label numbers correspond to description in text.

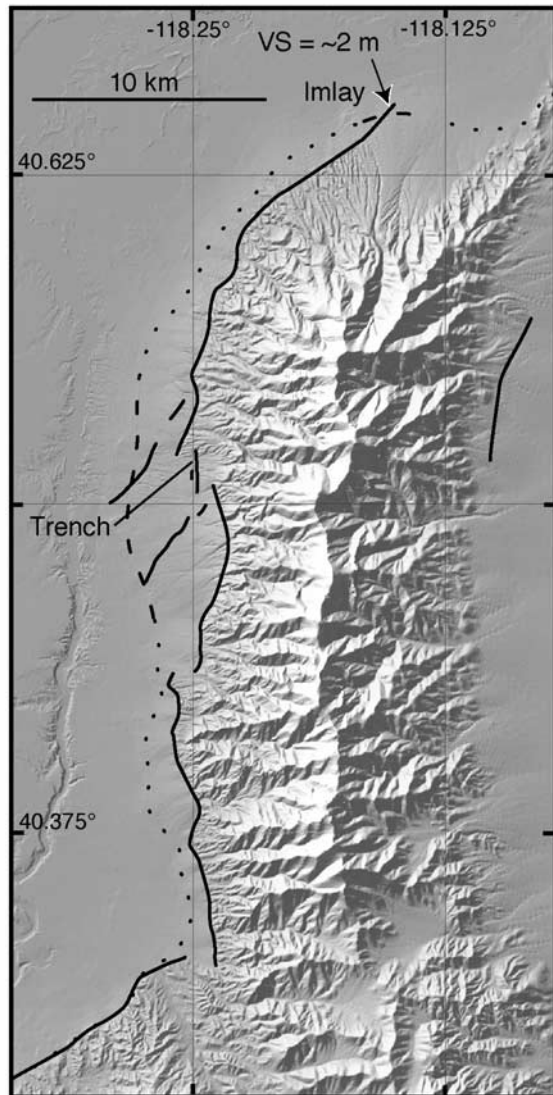


**Figure 10.** Fault trace (bold line) and trench locality along Humboldt Range. Highstand elevation of pluvial Lake Lahontan is dotted line where projected and bold dashed line where remnant lacustrine features remain well preserved. Vertical separations (VS) of post Lake Lahontan highstand surfaces across the fault are  $\sim 2$  m at the northern end of the fault trace. Fault is labeled 8 in Figure 2.

producing a fissure (unit 4) but little to no vertical offset across the fault at the trench. The event that produced the fissure is probably due to shaking and reactivation of the fault during the same earthquake that is recorded by  $\sim 2$  m vertical offsets of deposits below the highstand of Lake Lahontan that are observed elsewhere along strike and best preserved at the northern end of the fault trace (Figure 10 and 11a). The penultimate surface rupture earthquake is represented by the scarp-derived colluvium (unit 3) on the west side of the fault that sits upon unit 2. The maximum thickness of the penultimate scarp-derived colluvium (Figure 12) is the same as the vertical separation of the fault derived from scarp profiling (Figure 3b). The mea-

sure of vertical separation may overestimate the actual displacement due to possible warping or fault graben formation on the footwall (Figure 11). Regardless, the scarp at the trench site was formed during the penultimate

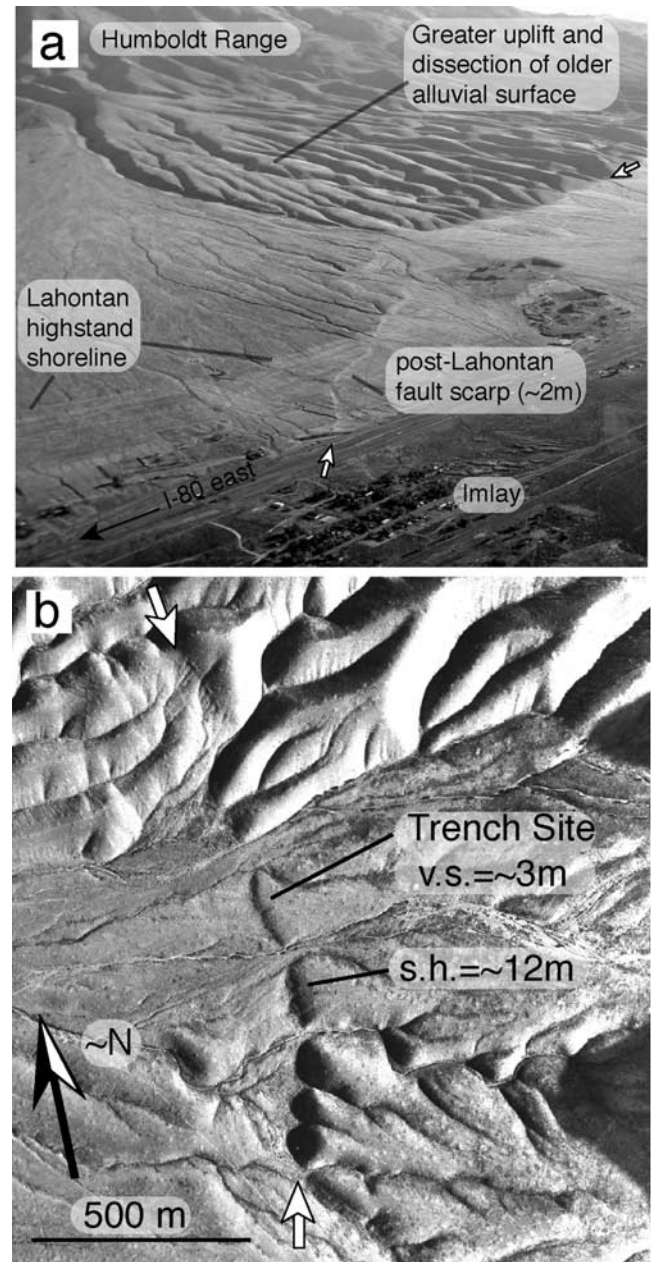


**Figure 11.** Morphological expressions of Quaternary displacement along fault-bounding west flank of Humboldt range. (a) Oblique air photo looking southward showing truncation and uplift of progressively older alluvial surfaces along northern end of fault (along white arrows) near Imlay (see Figure 10). Youngest displacement here also cuts highstand shorelines of pluvial Lake Lahontan. (b) Vertical air photo of scarp along Humboldt fault trace (between white arrows) in vicinity of trench site (see Figure 10). Repeated Quaternary movement on the fault is indicated by the increase in size of scarps (v.s., vertical separation; and s.h., scarp height) and higher elevation and greater incision of fault-bounded surfaces to the south of the trench site.

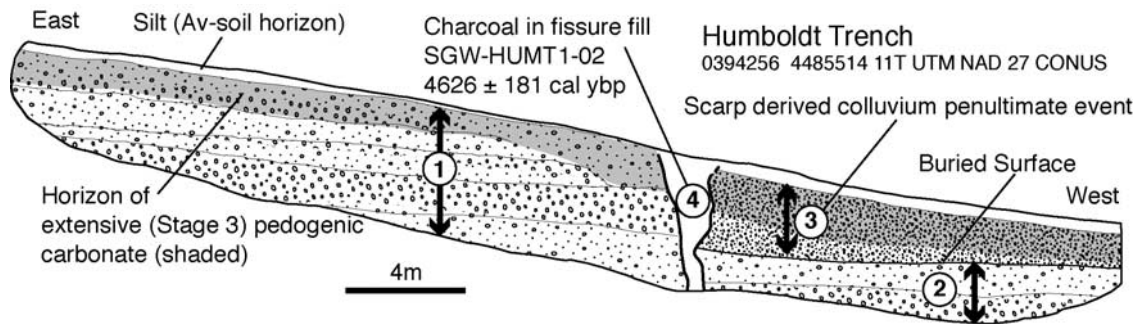


**Figure 12.** Sketch of trench exposure across Humboldt Range fault. Location is shown in Figures 10 and 11. Unit label numbers and shading correspond to description in text.

event and unit 2 was at the ground surface at that time. The apparent lack of a paleosol on the portion of unit 2 buried by scarp-derived colluvium of unit 3, and the similarity of soil development on the footwall (unit 1) and the scarp-derived colluvium (unit 3) suggests soil development for the most part postdates the scarp-forming event and formation of colluvial unit 3. Reconstruction of the cross section to remove the penultimate offset juxtaposes units 1 and 2. If individual beds in units 1 and 2 do not correlate across the fault displacement, the juxtaposition requires one or more events prior to the penultimate scarp-forming event.

[22] Because the most recent event produced negligible vertical offset at the trench site, the scarp may be reasonably approximated to be the result of a single earthquake displacement. A profile of the scarp surveyed adjacent to the trench and synthetic profiles constructed using the diffusion equation are shown in Figure 3b. The best fit of a synthetic curve to the observed is found for vertical scarp offset of 2.7 m and  $\kappa t = 35 \text{ m}^2$ . Assuming that the value of  $\kappa$  is in the range of 1, as put forth in the review of Hanks [2000] and suggested by the prior scarp analysis at the Blue Wing Mountain trench site, the scarp analysis suggests the penultimate and scarp forming earthquake occurred around 35 kyr ago.

**3.4. Sonoma Range**

[23] The Sonoma Range is an east tilted fault block composed primarily of lower Paleozoic to upper Triassic sedimentary rocks [Gilluly, 1967]. The range is the north-west continuation of the Tobin Range (Figure 13). The 1915 Pleasant Valley earthquake produced surface rupture along ~40 km of the west flank of the Tobin Range [Wallace, 1984a]. The earthquake is the northernmost of historical ruptures that define the central Nevada seismic belt. The trace of an active fault strikes along the west side of the Sonoma Range, producing scarps in late Pleistocene surfaces that have uplifted and created abandoned older fan surfaces. Faulting has produced ~1300 m of vertical relief between the valley floor and highest ridges which surpass ~2700 m. We placed a trench across a prominent trace of the fault preserved in fan sediments of probable late Pleistocene age outboard of Bacon Canyon (Figure 14).

[24] The Bacon Canyon trench log is shown in Figure 15. Distinct beds of subrounded to subangular pebble and cobble alluvial gravel are denoted as units 1, 2, and 3,

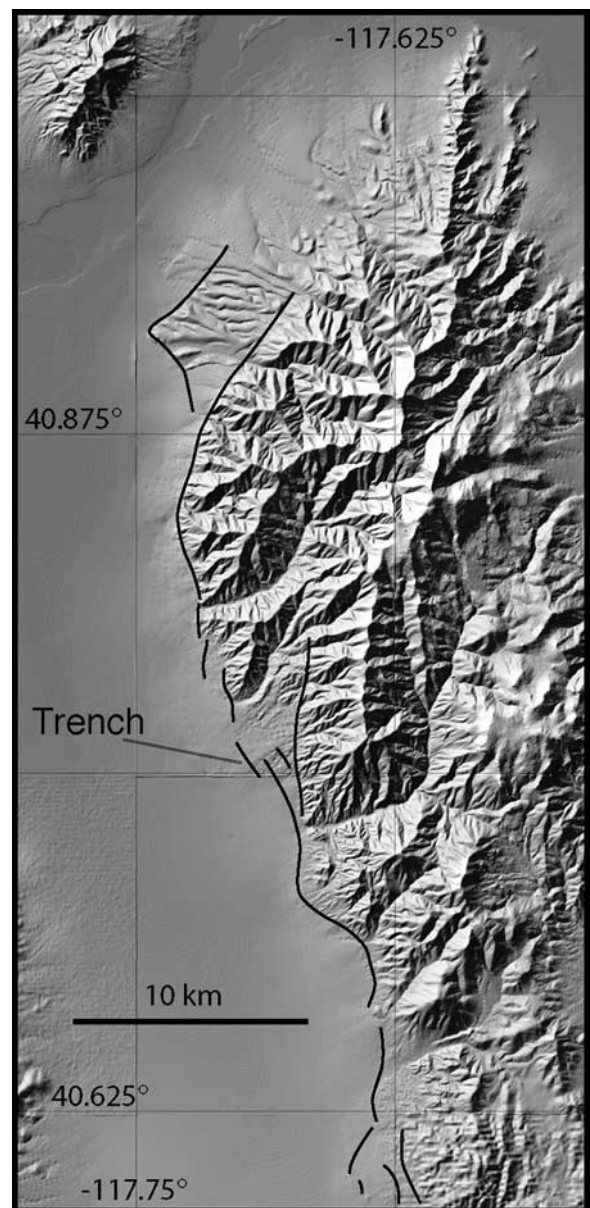


**Figure 13.** Sonoma Range active normal fault trace (solid lines) and trench location. Fault is labeled 11 in Figure 2.

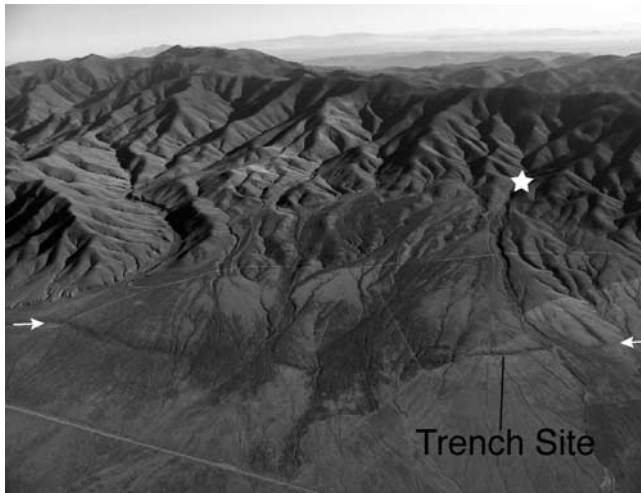


**Figure 14.** Trench site on active fault trace (between white arrows) along west flank of Sonoma Range near Bacon Canyon (star). A bedrock-alluvial scarp is also present at the range front in the background. View is to east. Location is annotated on map in Figure 13.

respectively. The units are broken by a fault that has produced a west facing scarp. Individual beds within hanging wall unit 2 are continuous across the length it is exposed and do not match those observed in unit 1 on the footwall. In contrast, unit 3 extends the length of the trench exposure and may be matched across the fault displacement. The base of unit 3 is offset  $\sim 4.5$  m across the fault. A significant portion of the offset is probably due to downwarping of units 2 and 3 near the fault trace. A triangular shaped package of scarp-derived colluvium (unit 4) rests upon the fault and the surface of unit 3 on the footwall. The colluvium is silt and fine sand with scattered pebbles and cobbles that decrease in concentration away from the fault and locally form a west dipping fabric. A rotated block or section of unit 3 and its capping soil is present at the base of the colluvial unit 4 (Figure 15). The block is interpreted to have been emplaced at the time of the scarp forming event. An AMS radiocarbon analysis of organic matter contained in a sample of the soil horizon resting on the rotated block gives a  $20,027 \pm 674$  cal years B.P. age for the sample (SGW-ST1-1, Table 1). Unit 4 is interpreted to represent a single period of colluviation subsequent to the displacement

of unit 3. The displacement of unit 3 across the fault is the same as the vertical separation of the ground surface across the fault and thus the top of unit 3 formed a continuous surface at the time of the displacement. From these observations it is inferred that the surface scarp is due to a single earthquake displacement that occurred near in time to the radiocarbon age  $20,027 \pm 674$  cal years B.P. Removing the 4.5 m of displacement produced at the fault by the earthquake juxtaposes units 1 and 2. The juxtaposition of the mismatched units records one or more prior events along the fault. The continuity of unit 3 across the fault that also occurs after removing the most recent displacement indicates that sufficient time passed for erosion to remove any scarp or scarp-derived colluvium produced by earlier events. The footwall unit 3 is overprinted by a stripped argillitic soil horizon and stage 3 carbonate development that extends to 2 m depth (shaded in Figure 15). On the hanging wall and beneath the fault derived colluvium of unit 4, unit 3 is overprinted by a paleosol that shares characteristics similar to those observed on the footwall; prominent oxidation, minor clay accumulation, and stage 3 carbonate development is 1–1.5 m thickness. The soil characteristics are consistent with the idea that the surface was stable for a relatively long period of time prior to the most recent scarp-forming earthquake.

[25] A survey of the scarp profile at the trench is compared in Figure 3c to synthetic profiles which best fit and bound the observed scarp profile. Vertical separation across the scarp is 2.4 m. The value of  $\kappa\tau$  that leads to the best fitting curve is  $18 \text{ m}^2$ . Dividing the best fitting value of  $\kappa\tau$  by the age of the scarp ( $\sim 20,000$  kyr) yields an estimate of  $\kappa = 0.9 \text{ m}^2 \text{ kyr}^{-1}$ , similar to the value found at the Blue Wing Mountain trench site and values reported for the Basin and Range by Hanks [2000].

### 3.5. Shoshone Range

[26] The northern Shoshone Range reaches elevations of  $>2800$  m above the adjacent valley fill at  $\sim 1400$  m elevation (Figure 16). The range consists primarily of Paleozoic rocks capped locally by east tilted Tertiary basalt [Stewart and McKee, 1977] and is bounded by an active normal fault on the west flank. Three trenches were excavated across the fault at Lewis Canyon where repeated Quaternary offset is recorded by progressively greater scarp heights across respectively older alluvial surfaces Q1, Q2, and Q3 (Figure 17). Sketches of the exposures are labeled 1, 2, and 3, respectively, and shown in Figure 18.

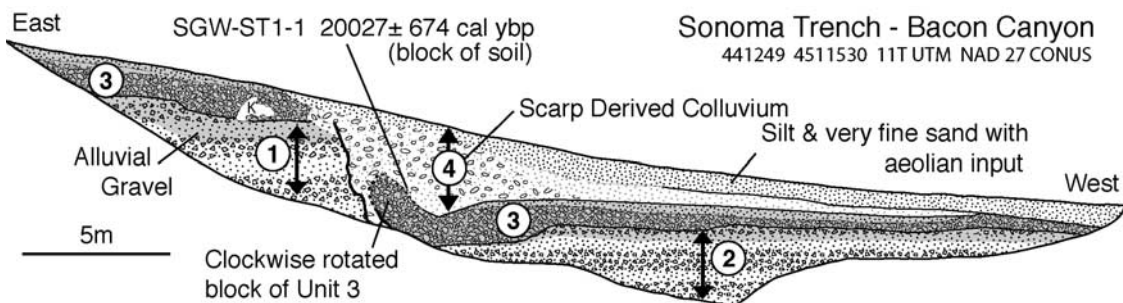


**Figure 15.** Sketch of trench exposure across Sonoma Range fault outboard of Bacon Canyon. Location is shown in Figures 13 and 14. Unit label numbers and shading correspond to description in text.

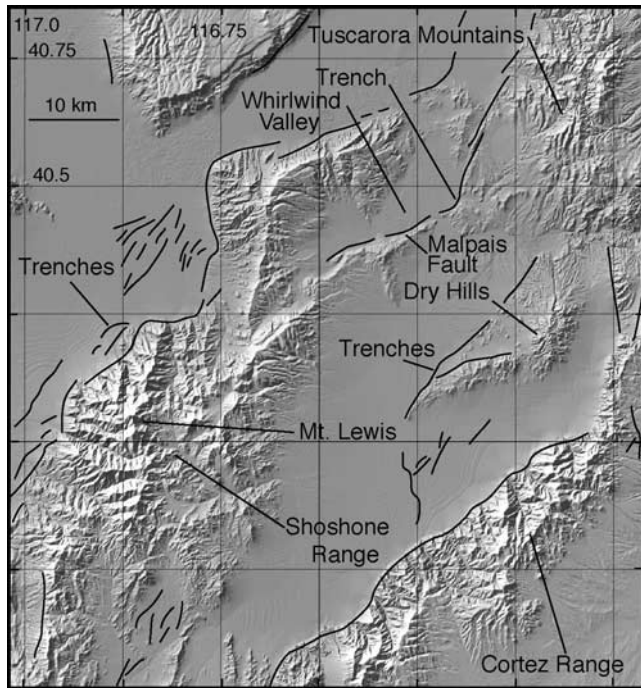


**Figure 16.** Active fault traces (solid lines) and locations of trench sites along the Shoshone Range, Tuscarora Mountains (Malpais Fault), and Dry Hills on shaded relief map. Faults are labeled 13, 14, and 15 in Figure 2.

Trench 1 was excavated across a  $\sim 0.4$  m scarp cutting the youngest alluvial fan surface Q1 (Figure 18a). The entire exposure consists of pebble and cobble alluvial gravel beds that are subhorizontal and continuous across the exposure except where offset by down-to-the-northwest fault displacement near the center of the exposure. The displacement in the subsurface is similar to the surface scarp height and, on that basis, interpreted to be the result of a single fault displacement. Analysis of a small charcoal sample taken from a bed at  $\sim 3$  m below the footwall surface indicates the displacement occurred subsequent to  $6867 \pm 119$  cal years B.P. (sample LCT-RC1-SGW, Table 1).

[27] The fault bifurcates to the northeast of trench 1 and cuts older alluvial surface Q2 (Figure 17). Soil on the Q2 surface exhibits a  $\sim 0.3$ -m-thick Bt horizon (clay) with strong columnar structure that overlies a zone of stage 3 pedogenic carbonate development. A sketch of the trench 2 exposure on the easternmost of the two strands is shown in Figure 18b. The section is cut by a normal fault that extends to the surface and dips steeply to the northwest. The oldest sedimentary layers are labeled unit 1. Unit 1 is subangular pebble and cobble alluvial gravel characterized by discontinuous beds that form a subhorizontal fabric. Though of similar fabric, an unambiguous match across the fault of layers internal to unit 1 in the foot and hanging wall was not observed. The upper contact of unit 1 on the footwall is downdropped  $\sim 1.7$  m from the surface across the fault. Unit 2 is a  $\sim 1.2$ -m-thick massive layer of silty sand and angular to subangular pebbles that is in fault contact and sits above unit 1 in the hanging wall. The upper portions of both units 1 and 2 on the foot and hanging wall, respectively, are overprinted by soil devel-

opment (Figure 18b). The degree of soil development on units 1 and 2 appears similar, though the expression of carbonate differs because of the difference in parent materials. Unit 3 is loosely compacted silt that fills a fault-bounded fissure and forms a wedge shape that thins to the northwest over the hanging wall. An Av silt soil horizon caps the entire exposure and is probably the main source of silt in fissure fill unit 3.

[28] The relations in trench 2 (Figure 18b) are interpreted to record at least two earthquake displacements. The fissure fill and colluvium of unit 3 was emplaced soon after the most recent displacement. In this regard, the top of unit 2 was the ground surface and continuous with the footwall surface at the time of the latest earthquake. The similarity of soil development on unit 1 to that on the buried portion of unit 2 are consistent with the interpretation. As well, the top of unit 2 is the ground surface to the northwest. Radiocarbon analysis of the organic fraction of the Av horizon that capped unit 2 at the time of the most recent event and that is now buried beneath unit 3 yields an age of  $3317 \pm 364$  cal years B.P. (sample LCT3-RC1, Table 1). From this we interpret that the most recent event occurred close to that time and simultaneously with the displacement recorded in trench 1. Additionally, the displacements registered during the most recent event are virtually identical in trench 1 and trench 2. The now faulted unit 2 is interpreted to be scarp-

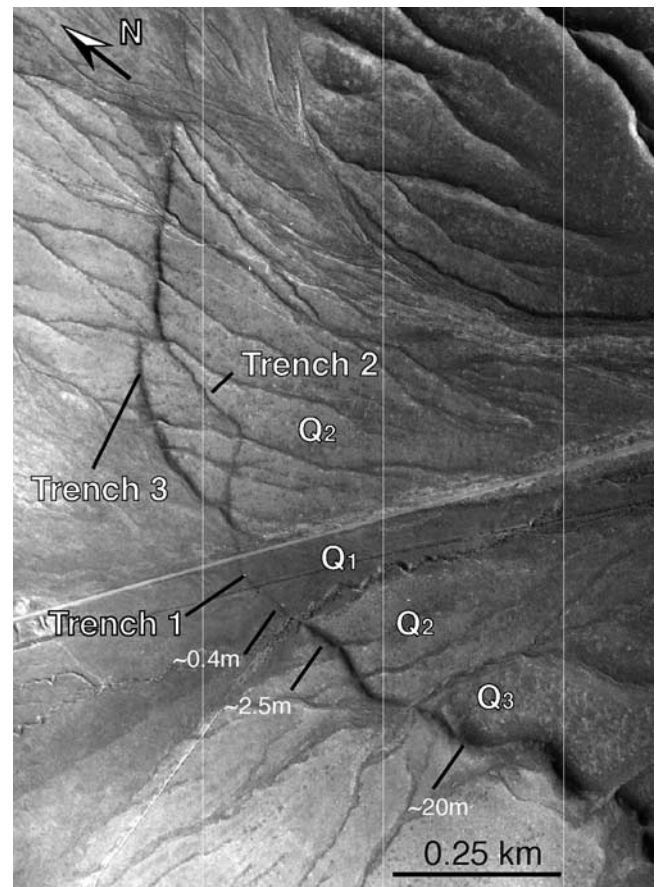


**Figure 17.** Vertical aerial photograph outboard of Lewis Canyon in the Shoshone Range shows trench site localities and progressively greater offsets of older alluvial surfaces Q1, Q2, and Q3, respectively. Scarp heights are in meters.

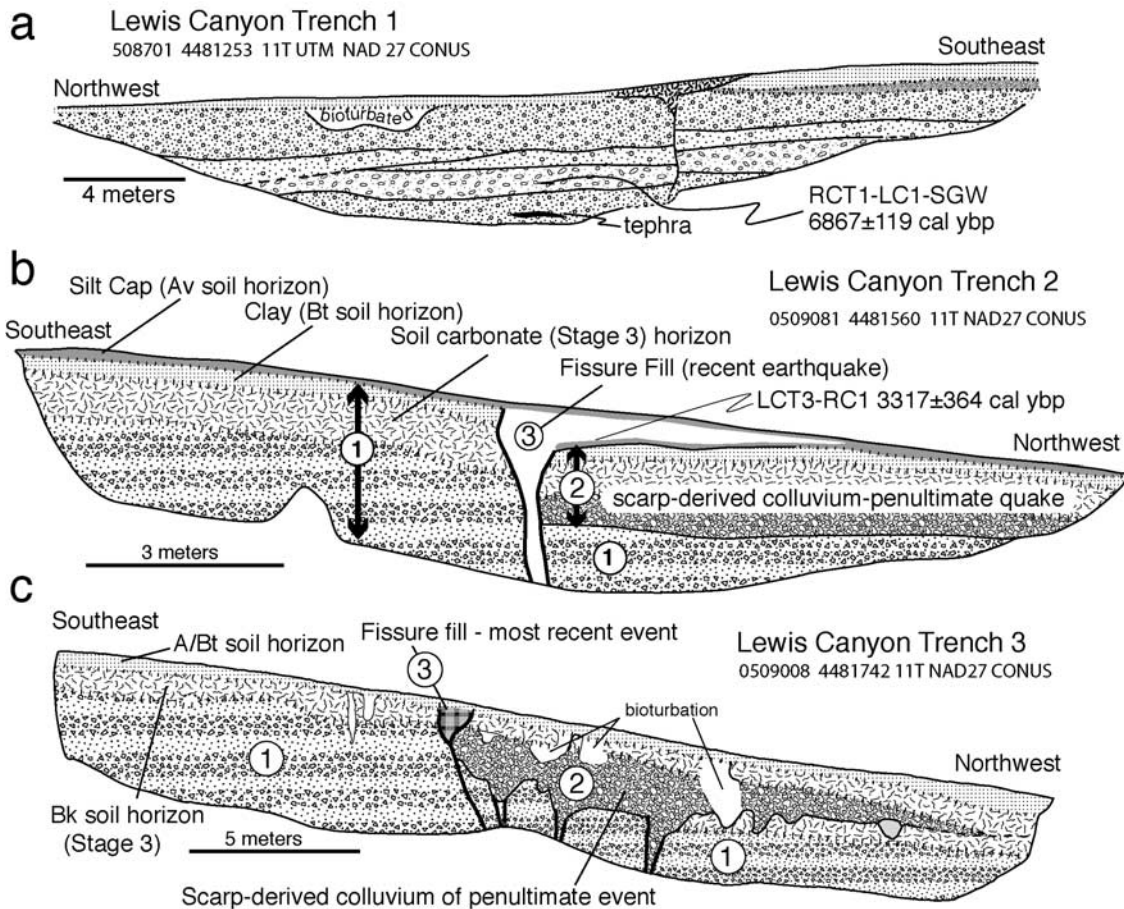


**Figure 18.** Sketches of trench exposures (a) 1, (b) 2, and (c) 3 across Shoshone Range fault at Lewis Canyon. Locations are shown in Figures 16 and 17. Unit label numbers and annotations correspond to description in text.

derived colluvium from a penultimate displacement, or possibly in part an alluvial deposit resulting from nearby incision and deposition on the hanging wall shortly after the penultimate event. The  $\sim 1.2$  m thickness of unit 2 provides an approximate bound on the vertical displacement during the penultimate event. Thus the penultimate earthquake displacement was greater than the most recent displacement along this fault strand. The possible mismatch of unit 1 in the foot and hanging wall allows the possibility of one or more prior events.

[29] The relations in trench 3 are similar to those observed in trench 2. Pebble and cobble alluvial gravel of unit 1 is faulted  $\sim 3$  m down to the northwest along the fault (Figure 18c). The top of the hanging wall portion of unit 1 becomes the ground surface to the west and is buried by the wedge-shaped unit 2 that is thickest at the fault and thins northwestward away from the fault. Unit 2 is massive silt and very fine sand with a 5–10% pebble component that decreases in concentration away from the fault, and is extensively bioturbated and permeated with pedogenic carbonate. The massive character and wedge shape of unit 2 is the basis to interpret that it is fault-derived colluvium. The argillitic Bt soil horizon and underlying stage 3 pedogenic carbonate development of a Bk soil horizon observed on the footwall of trench 3 extend across the length of the exposure (Figure 18c). The soil horizon-

ation thins slightly along the scarp and is disrupted by unit 3, a loose and massive silty sand that fills a fissure above the main trace of the fault. The fissure is interpreted to have occurred simultaneously with the most recent event recorded in adjacent trenches 1 and 2 ( $\sim 3317 \pm 364$  cal years B.P.) and filled by colluvial processes shortly thereafter. No vertical displacement accompanied the fissuring. The fault-derived colluvium of unit 2 is accordingly attributed to a penultimate displacement that occurred simultaneously with the penultimate displacement in trench 2. The scarp across which trench 3 is excavated may be attributed solely to displacement during the penultimate event and, in that regard, is a single-event fault scarp. Again, the lack of a clear match across the fault of layers within unit 1 on the footwall and hanging walls allows the possibility of one or more prior events.

[30] A survey of the trench 3 scarp profile is compared in Figure 3d to synthetic profiles which best fit and bound the observed scarp profile. Vertical offset of the surface across the scarp is 3.5 m. The synthetic curve that best fits the observed profile is found with vertical separation set to 3.5 m and of a value of  $\kappa t = 40$  m<sup>2</sup>. Given values of diffusivity  $\kappa$  are equal to  $\sim 1$  in the Basin and Range, the analysis suggests that the earthquake that produced the scarp at trench 3 occurred about 40,000 years B.P. In sum, the trenches and profile analysis reveal a history of two surface



**Figure 19.** Active fault trace (dashed white line) and trench site along eastern edge of Whirlwind Valley. View is to northwest. General location is indicated in Figure 16.

rupture events separated in time by many tens of thousands of years, with the most recent producing much less vertical slip (0.4 m) than the earlier ( $3.5 + 1.2 = 4.7$  m).

### 3.6. Tuscarora Mountains: Malpais Fault

[31] Whirlwind Valley is a structurally controlled valley on the northeast end of the Shoshone Range (Figure 16). The west side of the Valley is bounded by the southward continuation of the west dipping normal fault that bounds the Tuscarora Mountains. The section of the fault within Whirlwind Valley has been referred to as the Malpais fault [e.g., *Layman*, 1984]. A trench was excavated along the Malpais fault in Whirlwind Valley (Figures 16 and 19). A sketch of the exposure is given in Figure 20. The footwall unit 1 comprises beds of poorly sorted, angular pebble-cobble alluvial gravel that is overprinted by a stage 2+ pedogenic carbonate horizon and a cap of dark fine silt and sand that includes the A and B soil horizons. The footwall units are truncated by the southeastern of two main fault strands. Deposits similar but not identical to unit 1 are also located at the base of the trench between the two fault strands and on the footwall. Units 2, 3, 4, and 5 are limited to the hanging wall of the exposure. Unit 2 is massive silty sand with 5–10% angular pebble clasts distributed randomly. Unit 3 is sand and angular pebble gravel with a

few percent of small boulder size clasts. Unit 3 is poorly stratified with the coarser component decreasing to the northwest away from the fault. The upper  $\sim 0.4$  m of the unit displays a blocky structure, reddening of color, and is probably a buried paleosol. Unit 4 is silt and very fine sand with a minor percentage of angular pebble clasts. Units 2, 3, and 4 are each interpreted to be fault-derived colluvium and alluvium shed laterally from nearby gullies incised into the scarp and deposited subsequent to three separate earthquakes of respectively younger age. Unit 5 is modern fan alluvium emanating from a nearby gully that incises the scarp.

[32] Radiocarbon analysis of the organic fraction of a bulk sample (BEO1-03-SGW, Table 1) of fine sand displaying blocky structure interpreted to be soil on which unit 4 was deposited provides an age of  $7450 \pm 112$  cal years B.P. The same analysis of the organic fraction of a bulk sample of a clayey fine sand (BEO1-05-SGW, Table 1) within the underlying colluvial unit 3 yields an age of  $18701 \pm 582$  cal years B.P. Assuming the ages reflect the approximate time of earthquakes that led to genesis of colluvial units 3 and 4, the results suggest a return time of about 10,000 years between the last two surface rupture events. The thickness of the colluvial wedge units 3 and 4 at the fault are  $\sim 2$  m and  $\sim 0.7$  m, respectively. The thicknesses place a minimum bound on the vertical offset during the penultimate and most recent events, respectively.

### 3.7. Dry Hills

[33] The Dry Hills are an east tilted fault block of Mesozoic intrusive and volcanic rocks locally capped by Tertiary basalt [*Roberts et al.*, 1967]. Quaternary deposits on the west flank of the range are cut by the bounding west dipping fault (Figure 16). Repeated Quaternary displacement is recorded in the relatively greater offset of older Quaternary surfaces across the fault (Figure 21). The locations and sketches of the two trench exposures are shown in Figures 16 and 22, and labeled north and south, respectively. The Dry Hills north trench was emplaced across a  $\sim 0.2$ - to 0.3-m-high scarp that cuts the youngest alluvial surface in Figure 21. The entire exposure is discontinuous beds (unit 1) of silty fine sand and poorly sorted, angular to subangular pebble gravel (Figure 22). The beds are broken by two faults. The easternmost normal fault dips to the west and displaces beds  $\sim 0.3$  m. The western strands

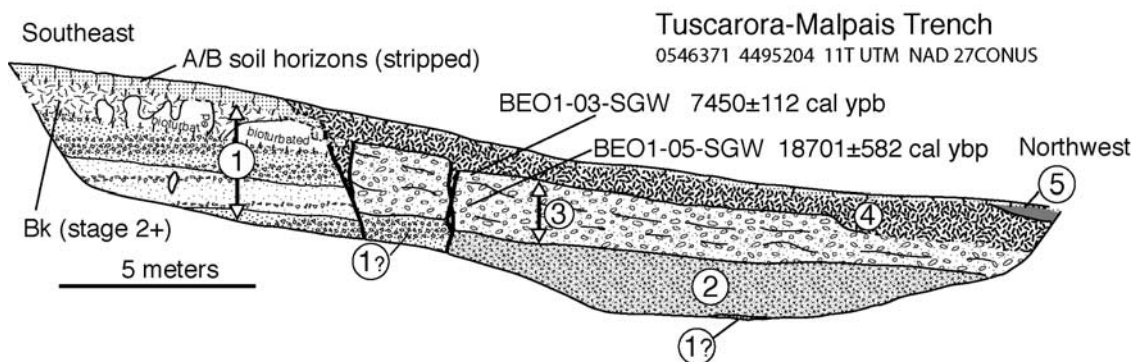


**Figure 20.** Sketch of trench exposure along Tuscarora-Malpais fault. Location is shown in Figures 16 and 19. Unit label numbers correspond to description in text.

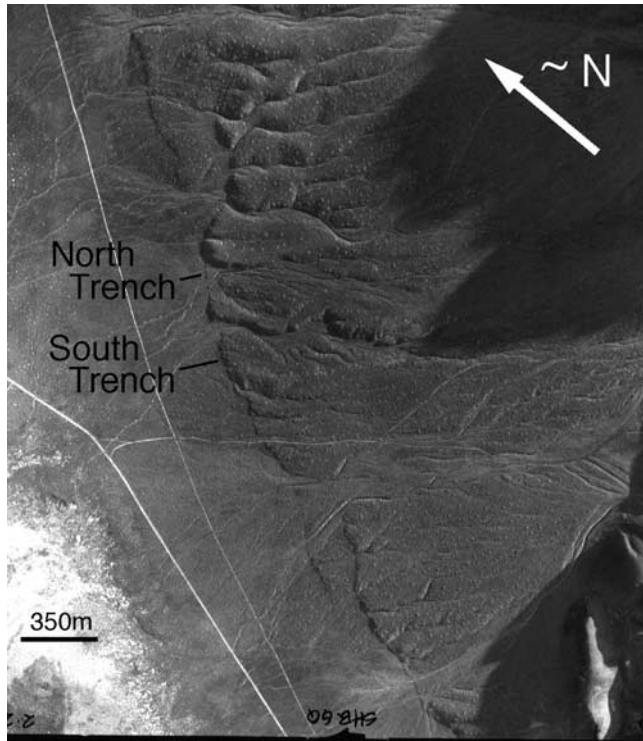


**Figure 21.** Vertical aerial photograph showing trace and trench sites along Dry Hills fault. General location is indicated in Figure 16.

bound a fissure. The entire exposure is capped by a layer of silt  $\sim 0.25$  m thick. Between the two fault strands and below the silt cap is massive, fine sand and silt with scattered angular pebbles interpreted to be fault-derived colluvium and fissure fill mixed with an aeolian component. Radiocarbon analysis shows the age of a charred seed of *Artemesia* (sagebrush) recovered from beneath the silt cap and within an undisturbed gravel layer on the footwall is  $5820 \pm 87$  cal years B.P. (DHT1-Bulk1, Table 1). The fault displacement occurred after and perhaps near in time to this age.

[34] The southern Dry Hills trench is placed across the trace where it cuts an older alluvial surface and displays a  $\sim 2$ -m-high scarp (Figure 21). The footwall is composed of massive light gray silt and very fine sand that displays distinct columnar blocky structure suggesting an additional clay component as well. The upper portion of unit 1 is extensively bioturbated. Soil on the surface is characterized by a weak B horizon of  $\sim 0.2$  m thickness and an underlying stage 2+ Bk horizon of about 0.5 m thickness. Unit 1 is not exposed in the hanging wall. The basal unit 2 in the hanging wall is very fine sand and subangular and angular pebble gravel showing cut and fill features and, hence, an alluvial origin. The upper  $\sim 0.2$  m of the unit is reddened very fine sand and interpreted to have previously been the ground surface. Unit 3 is also limited to the hanging wall. It is  $\sim 1.5$  m thick at the fault and thins to the west. The lower  $\sim 0.8$  m of unit 3 is massive, very fine sand and silt with a minor component of angular and subangular pebbles that decrease in concentration away from the fault. The upper third of the unit is overprinted by stage 2+ soil carbonate

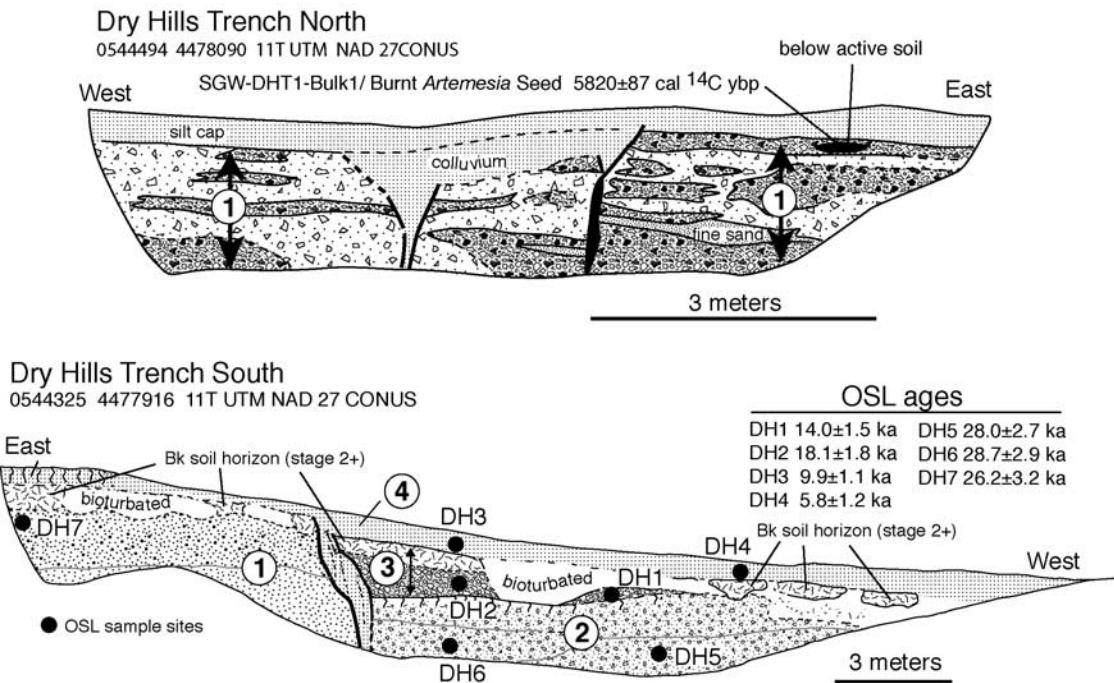


**Figure 22.** Sketches of (top) northern and (bottom) southern trench exposures across Dry Hills fault. Locations are given by UTM coordinates and shown in Figures 16 and 21. Unit label numbers correspond to discussion in text.

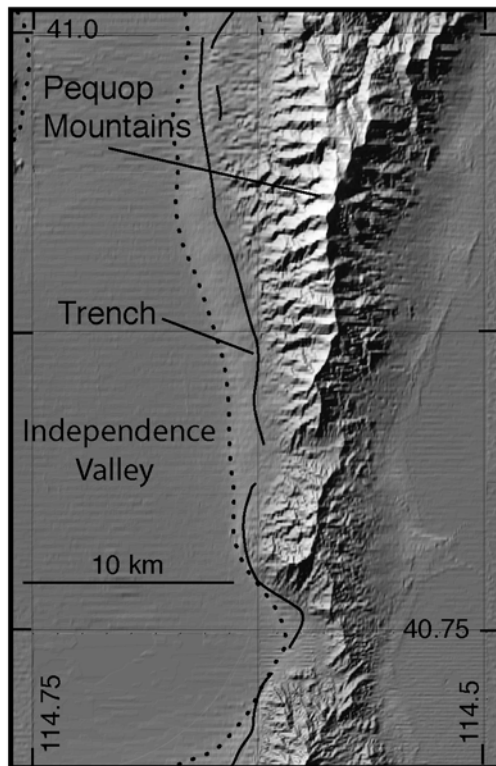


**Figure 23.** Pequop Range active normal fault trace and trench locality on shaded relief map. Dotted line traces highstand level of pluvial Lake Clover. Fault is labeled 18 in Figure 2.

development like that developed on unit 1 on the footwall. The observations are the basis to interpret unit 3 is fault-derived colluvium that also once marked the ground surface for a period of time. The  $\sim 1.5$  m thickness of unit 3 at the fault provides a minimum bound on the fault displacement that led to its development. Unit 3 is in turn displaced  $\sim 30$  cm downward from the footwall surface. Unit 4 is silt and very fine sand interpreted to be a mix of fault derived colluvium and aeolian input that filled the fissure and covered the scarp produced after unit 3 was displaced. In sum, colluvial units 3 and 4 are interpreted to have been deposited at the time of or shortly after two separate surface rupturing earthquakes. Displacement during the penultimate event was 4 to 5 times greater than the most recent. The faulting and absence of alluvial unit 2 on the footwall is also interpreted to record at least one yet earlier fault displacement.

[35] Each of the units in the southern Dry Hills trench was sampled and analyzed for age using optically stimulated luminescence. The resulting ages and sample numbers are listed in Figure 22. Colluvial unit 4 formed since the most recent displacement. The ages of two samples (DH3 and DH4) taken from the base of colluvial unit 4 are  $5.8 \pm 1.2$  ka and  $9.9 \pm 1.1$  ka. The youngest age is similar to that determined for the displacement recorded in the adjacent northern trench. Colluvial unit 3 is attributed to a penultimate earthquake displacement. Samples DH1 and DH2 taken from the colluvial unit 3 yield ages of  $14.0 \pm 1.5$  ka and  $18.1 \pm 1.8$  ka, respectively. The results indicate a period

of about 10,000 years separates the two most recent surface rupture events. Samples DH5 and DH6 are taken from faulted unit 2, give similar ages of about 28,000 ka that may approximate the age of a yet earlier fault displacement. Sample DH7 taken from the upper portion of footwall unit 1 gives a similar age to the samples collected in unit 2.

[36] When the observations of the two trenches are taken together, they lead to an interpretation of repeated surface ruptures of varying coseismic displacement separated in time by periods of time of about 10,000 years. The most recent surface rupture of about 30 cm normal displacement occurred at or after about 5,800 years ago, based on the radiocarbon age in trench 1. That event was preceded by another surface rupture event that produced a larger  $\sim 1.2$  m offset that occurred about 14 to 18 kyr ago, and perhaps another displacement event of similar size about 28 kyr ago.

### 3.8. Pequops

[37] An east tilted fault block constructed of Paleozoic carbonate and silici-clastic rocks [Coats, 1987], the Pequop Mountains reach an elevation of  $\sim 2800$  m relative to adjacent basins that sit at  $\sim 1700$  m elevation (Figure 23). The west flank is bounded by an active normal fault that dips west and is expressed as scarps in Quaternary deposits. Independence Valley on the west cradled the late Pleistocene pluvial Lake Clover [Reheis, 1999]. Erosional wave cut scarps and shoreline deposits of the highstand are preserved at  $\sim 1725$  m elevation and assumed here to correlate close in time to the  $\sim 15,500$  cal years B.P. highstand of Lake Lahontan [e.g., Adams and Wesnousky, 1998, 1999]. The modification of range-bounding fault scarps and alluvial deposits that cut the fault scarps by highstand shoreline features indicate that the last surface rupture event preceded the highstand of the lake. A location photo and sketch of a trench exposure on a scarp preserved above the highstand on a late Pleistocene alluvial surface are shown in Figures 24 and 25, respectively. Unit 1, the oldest deposit exposed, is subhorizontal discontinuous thin and medium beds of poorly sorted subangular pebble and cobble gravel. Unit 1 comprises the whole of the footwall exposure and is displaced downward  $\sim 3$  m to the west along a steep west dipping fault. Pedogenic carbonate locally reaching stage 4 development overprints the upper  $\sim 1$  m of unit 1 on the footwall. Unit 2 is a fault-bounded massive fine sand and silt layer with 1–2% subangular pebble clasts observed only on the hanging wall. It is  $\sim 0.5$  m thickness at the fault and thins to the west. Unit 3 is an assemblage of thin and medium discontinuous lenses of poorly sorted sand, pebble,



**Figure 24.** Photo of fault scarp and trench site viewed southward along west flank of Pequop Mountains.

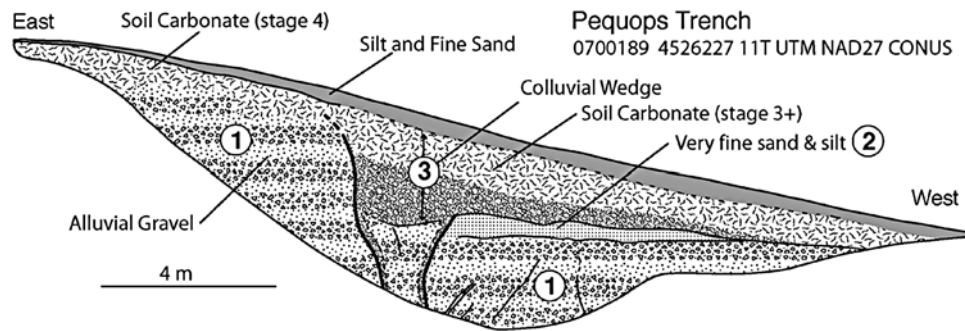


**Figure 25.** Sketch of trench exposure along Pequop Range normal fault. Location is shown in Figures 23 and 24. Unit label numbers correspond to discussion in text.

and small cobble gravel that impart a west dipping fabric to the unit. The deposit is  $\sim 3$  m thick at the fault, overprinted by stage 3+ pedogenic carbonate, thins westward, and the coarser component decreases upward and away from the fault. Unit 3 is on that basis interpreted to be fault derived colluvium. The genesis of faulted unit 2 is less clear. Unit 2 may be a mix of aeolian input and fault derived colluvium developed on a scarp that was small or for the most part eroded prior to the earthquake displacement responsible for the development of unit 3. As well, it may simply be a fine-grained capping layer on unit 1 unrelated to prior earthquake displacements. The observations that unit 1 on the hanging wall becomes the ground surface at the west end of the exposure and that the thickness of unit 3 at the fault is virtually the same as the vertical separation across the surface scarp are the basis to interpret that the scarp observed today is primarily due to single earthquake displacement.

[38] A survey of the scarp at the Pequops trench is compared in Figure 3e to synthetic profiles which best fit and bound the observed scarp profile. Vertical separation across the scarp is 2.9 m. The value of  $\kappa t$  that leads to the best fitting curve is  $42 \text{ m}^2$ . Again accepting that values of diffusivity  $\kappa$  are equal to  $\sim 1$  in the Basin and Range, and that the scarp is due to a single displacement, the analysis suggests that the earthquake that produced the scarp at trench 3 occurred about 42 ka and no surface ruptures have occurred since that time. The degree of soil development on colluvial unit 3 is consistent with the interpretation.

### 3.9. Previously Reported Observations

[39] Similar efforts have established the surface rupture history of faults elsewhere in the northern Great Basin. The results of those studies are here briefly recounted. The locations of faults and earthquake ruptures discussed are also labeled in Figure 2.

#### 3.9.1. Western Margin of Great Basin

[40] The Genoa fault is an east facing normal fault located within the transition between the Basin and Range faulting in the Great Basin and the Sierra Nevada. *Ramelli et al.* [1999] report the fault produced two large surface rupture events that each produced 3.0 to 5.5 m of dip slip at 500–600 cal years B.P. and 2000–2200 cal years B.P. The Peavine Peak fault is located just to the north. A trench emplaced across the northeast striking and east dipping fault provided *Ramelli et al.* [2004] evidence of right-oblique

motion on a northeast dipping fault and four to five surface rupture events during the last 6000–8000 years, with average oblique slip displacements estimated to be at least 1.5 to 2.0 m per event. *Wills and Borchardt* [1993] report that the Honey Lake strike-slip fault in California has produced at least four surface faulting earthquakes since  $\sim 6$  ka and slipped on average at 1.1 to 2.6  $\text{mm yr}^{-1}$  during the Holocene, based on study of an offset stream and exposure along a natural stream cut. *dePolo and Ramelli* [2003] interpret recent excavations across the Warm Springs strike-slip fault to indicate at least three surface rupture earthquakes during the last  $\sim 15,000$  years. The trenches and accompanying geomorphic analysis of *Briggs and Wesnousky* [2004] along the Pyramid Lake strike-slip fault similarly show at least four strike-slip surface rupture earthquakes post  $\sim 15,500$  cal years B.P. and a minimum fault slip rate of  $\sim 2$  to 3  $\text{mm yr}^{-1}$ . Direct evidence of the coseismic offset during the strike-slip events is not reported.

#### 3.9.2. Eastern Margin of Great Basin

[41] The  $\sim 350$ -km-long Wasatch Range front marks the easternmost extent of significant normal faulting in northern Great Basin. The paleoseismic history of the Wasatch range front fault has been studied extensively. A summary of those studies by *Machette et al.* [1992] shows sections of the Wasatch fault zone have produced surface ruptures on average each  $1980 \pm 310$  years during the last  $\sim 6000$  years. Intervent times between surface ruptures on sections of the fault between Brigham City and Salt Lake City, approximately at the latitude of the transect taken in this study, range from about 1300 to 1800 years [*McCalpin and Nishenko*, 1996], with vertical offsets commonly between 2 and 3 m [*Machette et al.*, 1992]. The East Great Salt Lake fault strikes parallel to the Wasatch range front. High-resolution seismic reflection profiles and cores within the Great Salt Lake show the East Great Salt Lake fault has produced at least three earthquakes with 3–5 m surface offsets since the dessication of Lake Bonneville about 13–14  $^{14}\text{C}$  ka [*Dinter and Pechman*, 2001, 2004]. The Oquirrh and South Oquirrh fault zones strike southward from the East Great Salt Lake fault. *Lund* [2004] reviews the studies of *Olig et al.* [2001] to interpret that five to seven surface rupture earthquakes have occurred along South Oquirrh fault zone during the last  $92 \pm 14$  kyr, and that the most recent three of the events probably also synchronously ruptured the Oquirrh fault. Study of the Stansbury – Skull Valley fault system points to slip rates on the order of

0.4 mm yr<sup>-1</sup> on the Stansbury fault but do not place limits on the age of individual paleoearthquake displacements [Swan *et al.*, 2004].

### 3.9.3. Interior of Great Basin

[42] Paleoearthquake studies within the interior of the Great Basin are currently few and scattered. *Wesnousky and Willoughby* [2003] interpret a trench exposure and soils to place the age of the last surface rupture earthquake along the northwest flank of the East Humboldt Range between 4800 and 7600 cal years B.P., preceded by tens of thousands of years or more of tectonic quiescence. A trench excavated by *Friederich et al.* [2004] across the normal fault bounding the west flank of the Cortez Range indicates a  $4.6 \pm 0.4$  m vertical displacement at  $2800 \pm 100$  cal years B.P. and no surface rupture for at least ~4000 years prior to that time. Similar study by *Machette et al.* [2002] of normal faults on the east flank of the Clan Alpine Range indicate two surface rupture events on the main range-bounding fault and three surface rupture events on an antithetic fault scarp located downslope about 1.6 km during the last ~130 kyr. The difference in earthquake records along the two faults is attributed to the possibility that the antithetic fault sometimes also slips in concert with the range-bounding fault along the west side of the Desatoya Mountains to the east. *Hanks and Wallace* [1985] have used crosscutting relationships and comparative scarp profiles to interpret the occurrence of one surface rupture event of 2.6–4.0 m vertical offset along the east flank of the Stillwater Range slightly before the highstand of pluvial Lake Lahontan ~15,500 cal years B.P. *Personius et al.* [2002] interpret trench exposures to indicate four surface ruptures along the normal fault bounding the west flank of the Santa Rosa Range since ~160 ka: 7–11 ka, 90–110 ka, 130–140 ka, and >140 ka, each producing 1–2 m of displacement.

### 3.9.4. Central Nevada Seismic Belt

[43] Trench exposures across strands of the 1932 Cedar Mountain earthquake led *Bell et al.* [1999] to interpret six surface rupture earthquakes during the last 32–36 kyr, including that in 1932. Best estimates of the pre-1932 ages are 4, 5, 12, 15, and 18 ka, each with  $\pm 2$  ka uncertainty, suggesting an average recurrence or interseismic interval of 3600 years. They further note that the net slip of 6–12 m for the six faulting events equates to a slip rate of 0.2 to 0.7 mm yr<sup>-1</sup>, with a preferred rate of 0.4–0.5 mm yr<sup>-1</sup>. In some contrast, observations just to the north along traces of the 1954 Fairview Peak earthquake rupture appear to indicate the Fairview fault had not ruptured for at least ~35 kyr prior to 1954 and is characterized by a slip rate of 0.1–0.2 mm yr<sup>-1</sup> [*Bell et al.*, 2004]. Within the “Bend” area near the northern extent of the 1954 Dixie Valley rupture, the trenching and chronostratigraphic study of *Bell and Katzer* [1990] place the occurrence of two pre-1954 surface rupture events: a penultimate event (The Bend event) at 2.0–2.5 <sup>14</sup>C ka [*Caskey et al.*, 2000] and a prior event that postdates alluvial fan deposits estimated to be 30–100 ka old. A longer-term vertical displacement rate of 0.2–0.5 mm yr<sup>-1</sup> is based on ~41 m offset of fan deposits estimated to be 200–500 ka. A trench across a ~5 m scarp at La Plata Canyon along the Sand Spring Range, immediately to the south and on strike of the 1954 Dixie Valley earthquake rupture, is reported by

*Bell et al.* [2004] to record three surface rupture events since 13.3 <sup>14</sup>C ka, with the most recent probably during the last 0.5–3.4 kyr, and an average minimum slip rate of about ~0.5 mm yr<sup>-1</sup>. To the west, the Rainbow Mountain and Fourmile Flat faults each produced surface rupture during the 1954 Rainbow Mountain–Fallon Stillwater earthquake sequence [*Tocher*, 1956]. *Caskey et al.* [2004] shows both faults also ruptured twice previously since about 17.8 <sup>14</sup>C ka. Prehistoric ruptures on the Rainbow Mountain fault are identified at 17.8–8.1 <sup>14</sup>C years B.P. and 9.9 to 6.3 <sup>14</sup>C years B.P. On the Fourmile Flat fault, it is plausible that the earliest of the prehistoric events coruptured with an event on the Rainbow Mountain fault, but the penultimate event of the sequence occurred subsequent to 1.5 ka. Post-latest Pleistocene net slip rates on the two faults are ~0.2–0.4 mm yr<sup>-1</sup> [*Caskey et al.*, 2004].

## 4. Discussion and Conclusion

[44] The ages of surface rupture on faults estimated in this study are summarized in Table 2. Also included in Table 2 are the previously described results of others from elsewhere in the northern Great Basin. The results of the studies are depicted in the space-time diagrams of Figures 2b and 2c. The horizontal axis of each plot is distance and plotted at the same scale as the underlying map in Figure 2a. The vertical axes are time. The numbers and letters along the horizontal axes correspond to faults on the underlying map in Figure 2a. Symbols plotted above the fault numbers denote the time of occurrence of a surface rupture earthquake on the respective fault. The length and continuity of the geologic record for each site is represented by the vertical dotted lines.

[45] Figure 2b is limited to faults north of about 40°N. Observations here extend westward across the entire Great Basin. The plot shows that the occurrence rate of surface rupture paleoearthquakes along ranges within the interior of the Great Basin is systematically less than observed along the margins. The pattern is similar to seismological and geodetic measurements that show background seismicity and strain accumulation is also concentrated along the margins of the Great Basin [e.g., *Bennett et al.*, 2003]. From this, we infer that the spatial variations of seismicity and strain accumulation observed across the northern Great Basin today have, to first order, been operative through the last 20–40 kyr or so. The inference assumes to first order that earthquake repeat time is a function of fault slip rate.

[46] The measured values of the vertical component of displacement for each paleoearthquake interpreted at trench sites during this study are annotated next to each event symbol in Figure 2b and summarized in Table 3. The vertical component of coseismic offsets vary from less than 1 m to greater than 4.5 m and are in the same range as observed along normal faults at the margins of the basin. For example, *Ramelli et al.* [2004] report paleoseismic dip-slip displacements of 3 to 5.5 m along the Genoa fault (fault 5 in Figure 2) along the western margin and *Machette et al.* [1991] infer the last few coseismic displacements along the Brigham segment of the Wasatch (northern part of fault 20 in Figure 2) were about 2 m. The similarity is consistent with the earlier assumption that the rate of strain release is to first order proportional to the occurrence rate

**Table 2.** Paleoseismic Synopsis

	Fault	Event Times <sup>a</sup>	Reference <sup>b</sup>
1	Honey Lake (SS)	>4 events since 5715 ± 65 cal years B.P.	a
2	Peavine	4–5 events in last 6000–8000 years	b
3	Warm Springs (SS)	at least 3 events in latest Pleistocene	c
4	Pyramid Lake (SS)	at least 4 events post ~15,500 cal years B.P.; most recent after 1705 ± 175 cal years B.P.	d
5	Genoa	2 events, 500–600 cal years B.P.; 2000–2200 cal years B.P.	e
6	Shawave-Blue Wing	1 event, 5453 ± 109 cal years B.P. (preferred); 1899–7777 cal years B.P. (limiting)	f
7	Hot Springs-Bradys	1 event, post ~15,500 cal years B.P.	f
8	Humboldt	2 events, 4626 ± 181 cal years B.P.; ~19 ka <sup>c</sup>	f
9	Santa Rosa	7–11 ka; 90–110 ka; 130–140 ka; >140–<160 ka	g
10	Stillwater	1 event, ~15–20 ka	h
11	Sonoma	1 event, ~20,027 ± 674 cal years B.P. (preferred)	f
12	Clan Alpine	2 or 3 events; post ~130 ka	i
13	Shoshone	2 events, ~3317 ± 364 cal years B.P.; ~40 ka <sup>c</sup>	f
14	Tuscarora-Malpais	2 events, ~7450 ± 112 cal years B.P.; ~1870 ± 582 cal years B.P. (preferred ages)	f
15	Dry Hills	3 events, ~5 ka (same as Cortez?); ~14–18 ka; ~28 ka	f
16	Cortez	1 event, 2800 ± 100 cal years B.P.; no event prior 6.4 ka	j
17	East Humboldt	1 event, 6200 ± 1400 cal years B.P., no event prior >10 ka	k
18	Pequop	1 event, ~28 ka <sup>c</sup>	f
19	East Great Salt Lake, Antelope segment	3 events, 586 +201/–241 cal years B.P.; 6170 +236/–234 cal years B.P.; 9898 +247/–302 cal years B.P.	l
19	East Great Salt Lake, Fremont segment	3 events, 3150 +235/–211 cal years B.P.; 6412 +209/–211 cal years B.P.; <11,427 +605/–449 cal years B.P. (average segment recurrence interval 4200 years)	l
20	Wasatch, Brigham segment	7 events, 2124 ± 104 cal years B.P.; 3434 ± 142 cal years B.P.; 4674 ± 108 cal years B.P.; 5970 ± 242 cal years B.P.; 7300 ± 350 cal years B.P.; 8518 ± 340 cal years B.P.; 13,010 cal years B.P. average segment recurrence interval ranges from ~1280 to ~1700 years on this and adjacent Weber segment	m
21	Wasatch, Provo segment	3 events, 618 ± 30 cal years B.P.; 2842 ± 72 cal years B.P.; 5481 ± 152 cal years B.P.; average segment recurrence interval ranges from ~2300 to 1900 on this and adjacent Nephi segment	m
22	Oquirrh	3 events, 4.8–7.9 cal kyr B.P.; 20.3–26.4 ka; >26.4 ka	s
23	South Oquirrh	5 events, 1.3–4.8 ka; 20–50 ka; <42 ± 8 ka; <75 ± 10 ka; near 92 ± 14 ka (youngest 3 may correlate to Oquirrh events)	s
24	Stansbury–Skull Valley	Late Quaternary slip rate ~0.4 mm yr <sup>-1</sup> , no ages for paleoearthquakes	t
B	1932 <i>M</i> 7.2 Cedar Mountain	6 events: 1932 A.D.; 4 ± 2 ka; 5 ± 2 ka; 12 ± 2 ka; 15 ± 2 ka; 18 ± 2 ka	n
C	1954 <i>M</i> 7.1 Fairview Peak	2 events: 1954 A.D.; >35 ka	or
D	1954 Dixie Valley (Bend) (La Plata Canyon)	3 events: 1954 A. D.; 2.0–2.5 ka; <35 ka	or
E	1954 <i>M</i> 6.8/6.6 Rainbow-Stillwater	3 events: 1954 A.D.; 6.3–9.9 ka; 8.1–17.8 ka (plus event at 0.0–1.5 ka on Fourmile Flat strand)	qr

<sup>a</sup>Surface rupture earthquake. Dendrochronologically corrected radiocarbon ages annotated cal years B.P. Uncorrected ages in thousands of years listed as ka.

<sup>b</sup>References: a, *Wills and Borchardt* [1993]; b, *Ramelli et al.* [2004]; c, *dePolo and Ramelli* [2003]; d, *Briggs and Wesnousky* [2004]; e, *Ramelli et al.* [1999]; f, this study; g, *Personius et al.* [2002]; h, *Hanks and Wallace* [1985]; i, *Machette et al.* [2002]; j, *Friedrich et al.* [2004]; k, *Wesnousky and Willoughby* [2003]; l, *Dinter and Pechman* [2000, 2001]; m, *McCalpin and Nishenko* [1996]; n, *Bell et al.* [1999]; o, *Caskey et al.* [2000]; p, *Bell and Katzer* [1990]; q, *Caskey et al.* [2004]; r, *Bell et al.* [2004]; s, *Lund* [2004]; t, *Swan et al.* [2004].

<sup>c</sup>Best estimate from scarp profiling. Uncertainty on order of 10 kyr.

of surface rupture earthquakes. When focusing attention on those sites where evidence of repeated offsets was observed, it is also evident that the amount of vertical offset registered from one event to the next is commonly very different. The Shoshone and Dry Hills sites are cases in point. For each, the most recent offset has been less than a half meter, whereas the penultimate events produced 4.7 and 1.5 m of vertical offset, respectively (Table 3).

[47] The localities in Figures 2a and 2b at latitudes between 40°N and 41°N and about 114°W and 119°W provide a transect of displacement observations that extends approximately east-west across and the interior of the Great Basin. The observations of vertical displacement for each paleoearthquake allow an estimate of the rate of horizontal extension across the northern Great Basin averaged over the

last 20–45 kyr. The vertical displacements and ensuing calculations are summarized in Table 3. We first make the initial simplifying assumption that all faults along the transect dip 60° at seismogenic depths. The assumption is in accord with the frictional considerations embodied in Andersonian mechanics [*Anderson, 1951*] as well as the steep dip of fault planes measured for large instrumentally recorded normal fault earthquakes in the Great Basin [e.g., *Doser, 1985, 1986*]. The horizontal extension *H* for each paleoearthquake is then equal to the measured vertical component of displacement (*V*) divided by the tan(60°). To resolve the calculated values of extension onto a common east-west azimuth (HEW), we multiply each value of *H* by the abs(cos(strike)), where strike is measured clockwise from north. In this manner, we calculate that the sum of

**Table 3.** Paleoearthquake Displacements

Fault	Vertical (V) Separation, <sup>a</sup> m	Extension (H) = V/tan(60°), m	Strike <sup>b</sup>	East-West Extension HEW, <sup>c</sup> m
<i>Post-45 ka</i>				
8, Humboldt	2.7(p)	1.6	180°	1.6
13, Shoshone	4.7(p and c), penultimate	2.7	210°	2.4
15, Dry Hills	1.5(c), triultimate	0.9	220°	0.7
18, Pequops	2.9(p)	1.7	0°	1.7
<i>Post-20 ka</i>				
6, Shawave (Bluewing)	3.3 (s and p)	1.9	30°	1.7
7, Brady–Hot Spring	2.0(s)	1.2	195°	1.1
8, Humboldt	2(p), recent	1.2	180°	1.2
9, Santa Rosa	1–2 <sup>d</sup>		190°	
10, Stillwater	2.6 <sup>e</sup> (p)	1.5	200°	1.4
11, Sonoma	2.4 (p and s)	1.4	150°	1.2
13, Shoshone	0.4(s), recent	0.2	220°	0.2
14, Tuscarora-Malpais	0.7(c), recent	0.4	200°	0.4
14, Tuscarora-Malpais	2(c), penultimate	1.2	200°	1.1
15, Dry Hills	0.3(s), recent	0.2	220°	0.1
15, Dry Hills	1.5(c), penultimate	0.9	220°	0.7
16, Cortez	4.6 <sup>f</sup> (s)	2.7	230°	1.7
17, East Humboldt	2.3 <sup>g</sup> (s)	1.3	195°	1.3
F, 1915 Pleasant Valley	2 <sup>h</sup> (a) (maximum 5.8)	1.2	200°	1.1
Sum	37.9	21.9 m		19.3
Sum (post-20 ka)	26.1	15.1 m		13.0

<sup>a</sup>Values assessed from (p) scarp profile, (c) colluvial wedge thickness, (s) stratigraphic offset, (a) average of surface slip distribution.

<sup>b</sup>Measured clockwise from north. Dip to right of strike direction.

<sup>c</sup>HEW = H \* Abs (cos(strike)).

<sup>d</sup>North of transect. Not included in sums.

<sup>e</sup>Hanks and Wallace [1985].

<sup>f</sup>Friederich et al. [2004].

<sup>g</sup>Wesnousky and Willoughby [2003].

<sup>h</sup>Wallace [1984a].

vertical displacements for paleoearthquakes along the transect during the last 45 kyr and 20 kyr are 37.9 m and 26.1 m, respectively (Table 3). The attendant total component of horizontal extension in the east-west direction (HEW) is then  $\sim 19.3$  m and  $\sim 13.0$  m, respectively. Dividing the extension by the time period over which displacement occurs yields values of extension rate across the transect equal to 19.3 m per 45 kyr = 0.42 mm yr<sup>-1</sup> and 13.0 m per 20 kyr = 0.65 mm yr<sup>-1</sup>. The relatively lesser value found when averaging over the longer 45 kyr period is probably the result of a less complete record of displacements (Figure 2b). The rates are equivalent to 1.0–1.6 nstrain yr<sup>-1</sup> easterly oriented extensional strain across the 400 km width of the transect. In comparison, the collinear GPS measurements of Bennett et al. [2003] between stations GOSH and GARL (Figure 1) indicate strain accumulation equivalent to about 2 mm yr<sup>-1</sup> of east-west extension. The uncertainties associated with the geologic estimate are many and warrant discussion.

[48] The geologically determined estimates of east-west extension rate are minimums when considering that earthquakes are likely missing from the record. The concern is somewhat tempered by the observation that our survey includes the major fault bounded mountain blocks across the transect (Figures 1 and 2) and that most of the paleoseismic records appear complete for the past  $\sim 20$  kyr. Even so, the single-event records obtained along the Shawaves, East Humboldts, Bradys and the Cortez range (faults 6, 7, 16, and 17 in Figure 2) do not preclude the occurrence of prior displacements over the 20 kyr and earlier time period. The trench studies and resulting estimates of displacement

are point measurements along the fault zones. One may reasonably question whether or not the particular offset measurements gleaned from the trenches are representative of the average offset in the paleoearthquakes. Large surface rupturing historical earthquakes in the Great Basin show considerable variation of surface slip along strike. The slip distributions of the 1983 Borah Peak [Crone et al., 1987] and 1954 Dixie Valley [Caskey et al., 1996] earthquakes are representative analogs and cases in point. Somewhat analogously, it is also possible that particular trench sites measure overlapping ruptures that principally broke separate sections of the same fault, in which case the contribution of a particular fault to the rate calculation may be overestimated. The problems while real may be somewhat moderated by the approach of summing offsets from many earthquakes on different faults and our attempt to site trenches where the most recent scarps are most prominent, thus yielding some measures that are greater and others that are less than the average offset associated with a particular fault or paleoearthquake. The extension rate estimate is also a minimum bound when considering that colluvial wedge thicknesses are directly used to estimate the offset of a number of the events in Table 3. A general first approximation that has been put forth is that the maximum thickness of scarp-derived colluvium is limited to half the height of the free face from which it was shed, though it has also been suggested that maximum wedge thickness may range from 0 to 100% on steeper slopes (e.g., see discussion of McCalpin [1996]). The extension rate estimate also ignores the potential contribution of lesser nonsurface rupturing earthquakes and aseismic

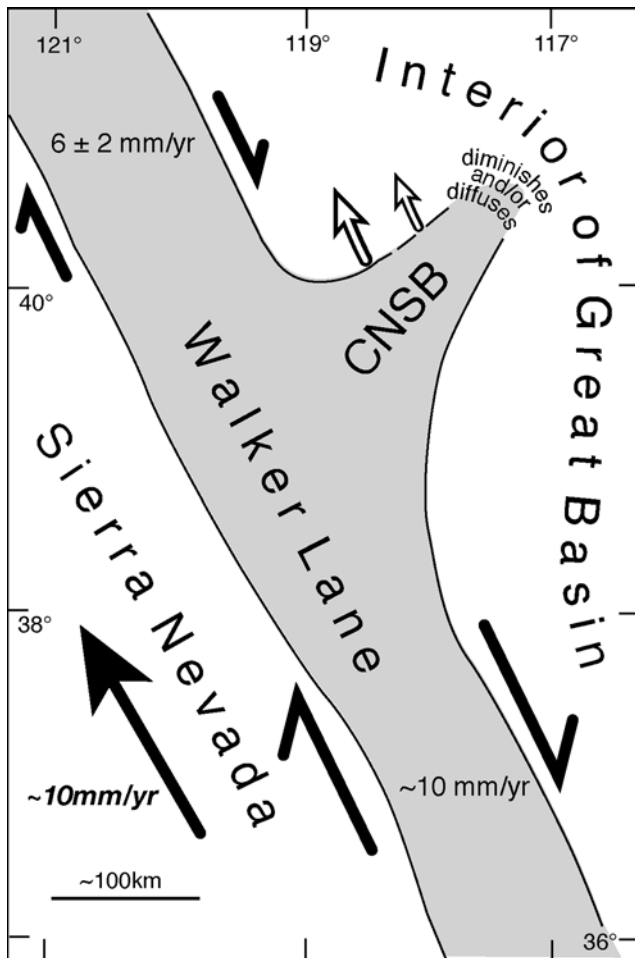


**Figure 26.** Schematic illustration of area of central Nevada seismic belt (CNSB) as a reentrant of relatively high strain rate extending northeast from the Walker Lane into the relatively rigid or slower deforming interior of the Great Basin. Areas of relatively high strain rate are shaded. Geodesy shows Walker Lane parallel motion of the Sierra Nevada with respect to the interior of the Great Basin to the east of  $117^{\circ}$  which is  $\sim 10 \text{ mm yr}^{-1}$  (large solid arrows [Bennett et al., 2003]). Most of that motion is observed as right-lateral northwest directed shear confined to the Walker Lane south of the CNSB (large oppositely facing half-sided arrows [Dixon et al., 1995; Gan et al., 2000]). Rates of geodetically observed strain accumulation across the northern Walker Lane are less ( $\sim 6 \pm 2 \text{ mm yr}^{-1}$ ) than observed to the south (smaller half-sided arrows [Thatcher et al., 1999]). Extension in the CNSB may play a role in the observed decrease by imparting a northward relative motion (open arrows) of the area northwest of the CNSB with respect to the southeast, resulting in a lesser relative right-lateral shear across the Walker Lane to the north of the CNSB.

creep, though it is generally accepted that the largest earthquakes account for most deformation [Brune, 1968] and we are aware of no documented accounts of aseismic fault slip for normal faults. Uncertainty is also coupled to the assumption of fault dip. For example, the assumption that all faults dip at a low angle of  $30^{\circ}$  rather than  $60^{\circ}$  would increase the extension rate estimate threefold. The

possibility of slip on low-angle normal faults exists [e.g., Caskey et al., 2000; Wesnousky and Willoughby, 2003], though a systematic bias of the data in this manner appears unlikely in light of observations that show major historical normal displacement earthquakes have ruptured on steeper fault planes with dips of  $\sim 50^{\circ}$ – $70^{\circ}$  [Doser, 1985, 1986]. In contrast to the prior uncertainties that would generally lead to the calculation of a minimum bound on the extension rate, there are competing factors that tend to yield an overestimate. For example, vertical near-surface displacements across and near normal faults are commonly greater than the actual vertical separation of footwall and hanging wall surfaces because of local warping or graben formation at the fault [e.g., see McCalpin, 1996]. While this effect can generally be taken into account with trench exposures and surveying for most recent events, it is more difficult to identify and take into account for penultimate and older events, in which case measures of colluvial wedge thicknesses may well overestimate the actual vertical ground displacement. A yet more significant factor that likely leads to a considerable overestimate rather than an underestimate of the calculated rates is the simplified method of calculation which effectively sums the displacements onto a single fault. A more rigorous and quantifiable geologic estimate of the late Pleistocene extension rate computed here will necessarily await documentation, if possible, of the slip distributions of past paleoearthquakes along these and other ranges and, for example, use of Kostrov's [1974] method to calculate volumetric strain, or systematic documentation and dating of fault-displaced Quaternary surfaces along the transect.

[49] Observations to the south of  $40^{\circ}$ N are provided in Figure 2c and also encompass the central Nevada seismic belt. The central Nevada seismic belt is defined by an alignment of historical surface rupture earthquakes (Figures 1 and 2a) and an increase in geodetic strain accumulation relative to the interior of the Great Basin to the east [e.g., Thatcher, 2003]. Examination of Figure 2c shows that the frequency of occurrence of latest Pleistocene and Holocene surface rupture earthquakes within the central Nevada seismic belt is characteristically greater than observed along ranges within the interior of the Great Basin to the north (Figure 2b). Paleoseismic data to the east and interior of the Great Basin are currently limited to Machette et al.'s [2002] interpretation of three events during the last  $\sim 130 \text{ k}$  along the Clan Alpine fault (Figure 2c), generally less frequent than for those faults in the central Nevada seismic belt. The regional active fault and fold database of the U.S. Geological Survey (USGS) [Haller et al., 2004; <http://qfaults.cr.usgs.gov>] reports that the last displacements on active faults east of the Clan Alpine fault (Figure 2a), within the interior of the Great Basin, and along the GPS transect of the USGS (Figure 1) generally occurred prior to the Holocene, suggesting they also are characterized by long recurrence times compared to faults within the central Nevada seismic belt. Assuming again that the rate of surface rupture earthquake recurrence is proportional to the rate of strain release, the recurrence pattern manifest in Figures 2b and 2c lead to the suggestion that the relatively higher level of late Pleistocene strain release which is localized in the central Nevada seismic belt diminishes or becomes less localized northward. The resulting implication

is that the spatial clustering of earthquakes that mark the central Nevada seismic belt has occurred in a region that has experienced relatively greater strain accumulation and release through the latest Pleistocene and Holocene as compared to surrounding areas of the Great Basin. The interpretations are further suggested when noting that the 0.4–0.7 mm yr<sup>-1</sup> extension rate calculated across the 400 km transect to the north of 40°N is at most equal to the geologically determined net extension rate 0.6–1.1 mm yr<sup>-1</sup> calculated by Bell *et al.* [2004] across the narrow width of the central Nevada seismic belt to the south of 40°N. Thus, while the historical alignment of surface ruptures that defines the central Nevada seismic belt reflects a unique clustering of earthquakes in time and space, it is perhaps less surprising that this historical cluster of ruptures would occur within the central Nevada seismic belt rather than to the east or northward in the interior of the Great Basin. We suggest that the central Nevada seismic belt be viewed over the latest Pleistocene as a reentrant of relatively high strain rate that strikes northeastward from the Walker Lane into the relatively rigid or slower deforming interior of the Great Basin (Figure 26). The reentrant of high strain rate may play a role in the observed difference in geodetically observed rates of northwest directed right-lateral shear observed to the northwest and southeast, respectively, of the Walker Lane intersection with the central Nevada seismic belt (Figure 26). The likelihood that this pattern of strain accumulation has been active over longer periods of time is addressed by Wesnousky [2005].

[50] **Acknowledgments.** A number of individuals visited one or more of the various field sites in this study. We thank them for their time and input: Tony Crone, Craig DePolo, Kathy Haller, Steve Personius, Mike Machette, Alan Ramelli, Tom Rennie, and Gordon Seitz. Wayne Thatcher's geodetic studies helped provide justification to allow this work. We thank him for that and valuable insight during the course of this study. Thanks are also extended to Isabelle Manighetti, Jerome Van Der Woerd, Ron Bruhn, and an anonymous reviewer for their detailed reviews leading to an improved manuscript. I thank IGNS and particularly Kelvin Berryman, Mark Stirling, and Terry Webb for providing facilities to complete the final stages of the manuscript. Frank Sullivan, Lee Loudon, Jim Navco, and Brad Quilici kindly lent technical expertise to the study. The hospitality of Lee and Nancy Loudon was most appreciated while working in Crescent Valley. Several of the sites were used as field exercises for graduate mapping classes. The senior author expresses thanks to NSF for the opportunity to bring the research experience into the classroom. This manuscript is based upon work supported by the National Science Foundation under Grant No. 0086667. Center for Neotectonic Studies Contribution No. 46.

## References

- Adams, K. D., and S. G. Wesnousky (1998), Shoreline processes and the age of the Lake Lahontan highstand in the Jessup embayment, Nevada, *Geol. Soc. Am. Bull.*, *110*, 1318–1332.
- Adams, K. D., and S. G. Wesnousky (1999), Surficial characteristics, soil development, and regional Shoreline correlation, *Geomorphology*, *30*, 357–392.
- Anderson, E. M. (1951), *The Dynamics of Faulting*, 206 pp., Oliver and Boyd, Edinburgh.
- Anderson, K., S. Wells, and R. Graham (2002), Pedogenesis of vesicular horizons, Cima volcanic field, Mojave Desert, California, *Soil Sci. Soc. Am. J.*, *66*, 878–887.
- Axelrod, D. J. (1956), Mio-Pliocene floras from west-central Nevada, *Univ. Calif. Publ. Geol. Sci.*, *33*, 322 pp.
- Bell, J. W., and T. Katzner (1990), Timing of late Quaternary faulting in the 1954 Dixie Valley earthquake area, central Nevada, *Geology*, *18*, 622–625.
- Bell, J. W., C. M. dePolo, A. R. Ramelli, A. M. Sarna-Wojcicki, and C. E. Meyer (1999), Surface faulting and paleoseismic history of the 1932 Cedar Mountain earthquake area, west-central Nevada, and implications for modern tectonics of the Walker Lane, *Geol. Soc. Am. Bull.*, *111*, 791–807.
- Bell, J. W., S. J. Caskey, A. R. Ramelli, and L. Guerrieri (2004), Pattern and rates of faulting in the central Nevada seismic belt and paleoseismic evidence for prior belt-like behavior, *Bull. Seismol. Soc. Am.*, *94*, 1229–1254, doi:10.1785/0120032226.
- Bennett, R. A., B. P. Wernicke, and J. L. Davis (1998), Continuous GPS measurements of contemporary deformation across the northern Basin and Range province, *Geophys. Res. Lett.*, *25*, 563–566.
- Bennett, R. A., B. P. Wernicke, N. A. Niemi, A. M. Friedrich, and J. L. Davis (2003), Contemporary strain rates in the northern Basin and Range province from GPS data, *Tectonics*, *22*(2), 1008, doi:10.1029/2001TC001355.
- Birkeland, P. (1999), *Soils and Geomorphology*, 432 pp., Oxford Univ. Press.
- Briggs, R. W., and S. G. Wesnousky (2004), Late Pleistocene fault slip rate, earthquake recurrence, and recency of slip along the Pyramid Lake fault zone, northern Walker Lane, United States, *J. Geophys. Res.*, *109*, B08402, doi:10.1029/2003JB002717.
- Brune, J. N. (1968), Seismic moment, seismicity, and rate of slip along major fault zones, *J. Geophys. Res.*, *73*, 777–784.
- Bucknam, R. C., and R. E. Anderson (1979), Estimation of fault-scarp ages from a scarp-height-slope-angle relationship, *Geology*, *7*, 11–14.
- Caskey, S. J., S. G. Wesnousky, P. Zhang, and D. B. Slemmons (1996), Surface faulting of the 1954 ( $M_s = 7.2$ ) and Dixie Valley ( $M_s = 6.8$ ) earthquakes, central Nevada, *Bull. Seismol. Soc. Am.*, *86*, 761–787.
- Caskey, S. J., J. W. Bell, D. B. Slemmons, and A. R. Ramelli (2000), Historical surface faulting and paleoseismology of the central Nevada seismic belt, in *Great Basin and Sierra Nevada, GSA Field Guide*, vol. 2, edited by D. R. Lageson, S. G. Peters, and M. M. Lahren, pp. 23–44, Geol. Soc. of Am., Boulder, Colo.
- Caskey, S. J., J. W. Bell, and S. G. Wesnousky (2004), Historic surface faulting and paleoseismicity in the area of the 1954 Rainbow Mountain–Stillwater earthquake sequence, *Bull. Seismol. Soc. Am.*, *94*, 1255–1275, doi:10.1785/012003012.
- Coats, R. R. (1987), Geology of Elko County, Nevada (1:250,000 scale map), *Nev. Bur. Mines Geol. Bull.*, *101*, 1–112.
- Crone, A. J., M. N. Machette, M. G. Bonilla, J. J. Lienkaemper, J. J. Pierce, W. E. Scott, and R. C. Bucknam (1987), Surface faulting accompanying the Borah Peak earthquake and segmentation of the Lost River fault, central Idaho, *Bull. Seismol. Soc. Am.*, *77*, 739–770.
- DeMets, C., and T. H. Dixon (1999), New kinematic models for Pacific–North America motion from 3 Ma to present: I. Evidence for steady motion and biases in the NUVEL-1A model, *Geophys. Res. Lett.*, *26*, 1921–1924.
- dePolo, C. M., and A. R. Ramelli (2003), The Warm Springs Valley fault system, A major right-lateral fault of the northern Walker Lane, western Nevada, paper presented at XVI INQUA Congress: Paleoseismology in the Twenty-first Century, A Global Perspective, Session 19, Int. Union for Quat. Res., Reno, Nev.
- Dinter, D. A., and J. C. Pechman (2000), Paleoseismology of the East Great Salt Lake Fault, USGS NHERP Final Project Summary, USGS Award Number: 98–HQ-GR-1013, U.S. Geol. Surv., Reston, Va.
- Dinter, D. A., and J. C. Pechman (2001), Seismic risk in the Wasatch Front region, Utah, from the East Great Salt Lake normal fault, estimates from high-resolution seismic reflection data, *Geol. Soc. Am. Abstr. Programs*, *33*(6), 346.
- Dinter, D. A., and J. C. Pechman (2004), Holocene segmentation and displacement history of the East Great Salt Lake fault, Utah, in *Basin and Range Province: Seismic Hazards Summit*, pp. 82–86, Nev. Bur. of Mines and Geol., Reno.
- Dixon, T. H., S. Robaudo, J. Lee, and M. C. Reheis (1995), Constraints on present-day Basin and Range deformation from space geodesy, *Tectonics*, *14*, 755–772.
- Dohernwend, J. C., B. A. Schell, C. M. Menges, B. C. Moring, and M. A. McKittrick (1996), Reconnaissance photogeologic map of young (Quaternary and Late Tertiary) faults in Nevada, *Nev. Bur. Mines Geol. Open File Rep.*, *96-2*, Plate 9-1, scale 1:1,000,000.
- Dokka, R. K., and C. J. Travis (1990), Role of the Eastern California Shear Zone in accommodating Pacific–North American plate motion, *Geophys. Res. Lett.*, *17*, 1323–1326.
- Doser, D. I. (1985), Source parameters and faulting processes of the 1959 Hebgen Lake, Montana, earthquake sequence, *J. Geophys. Res.*, *90*, 4537–4555.
- Doser, D. I. (1986), Earthquake processes in the Rainbow Mountain–Fairview Peak–Dixie Valley, Nevada, region 1954–1959, *J. Geophys. Res.*, *91*, 12,572–12,586.
- Friedrich, A. M., J. Lee, B. P. Wernicke, and K. Sieh (2004), Geologic context of geodetic data across a Basin and Range normal fault, Crescent Valley, Nevada, *Tectonics*, *23*, TC2015, doi:10.1029/2003TC001528.

- Gilluly, J. (1967), Geologic map of the Winnemucca quadrangle, Pershing and Humboldt Counties, Nevada, *U.S. Geol. Surv. Quadrangle Map, GQ-656*, scale 1:62,500.
- Goter, S. K., G. P. Thelin, and R. J. Pike (1992), Earthquakes in the conterminous United States, U.S. Geol. Surv., Natl. Earthquake Inf. Cent., Boulder, Colo.
- Goter, S. K., D. H. Oppenheimer, J. J. Mori, M. Savage, and R. Masse (1994), Earthquakes in California and Nevada, *U.S. Geol. Surv. Open File Rep., 94-647*, scale 1:1,000,000.
- Haller, K. M., M. N. Machette, R. L. Dart, and B. S. Rhea (2004), U.S. Quaternary fault and fold database released, *Eos*, 85(22), 218.
- Hammond, W. C., and W. Thatcher (2004), Contemporary tectonic deformation of the Basin and Range province, western United States: 10 years of observation with the Global Positioning System, *J. Geophys. Res.*, 109, B08403, doi:10.1029/2003JB002746.
- Hanks, T. C. (2000), The age of scarplike landforms from diffusion-equation analysis, in *Quaternary Geochronology: Methods and Applications, Ref. Shelf*, vol. 4, edited by J. S. Noller, J. M. Sowers, and W. R. Lettis, pp. 313–338, AGU, Washington, D. C.
- Hanks, T. C., and D. J. Andrews (1989), Effect of far-field slope on morphologic dating of scarplike landforms, *J. Geophys. Res.*, 94, 565–573.
- Hanks, T. C., and R. E. Wallace (1985), Morphological analysis of the Lake Lahontan shoreline and beachfront fault scarps, Pershing County, Nevada, *Bull. Seismol. Soc. Am.*, 75, 835–846.
- Harden, J. W. (1982), A quantitative index of soil development from field descriptions: Examples from a chronosequence in central California, *Geoderma*, 28, 1–23.
- Hetland, E. A., and B. H. Hager (2003), Postseismic relaxation across the Central Nevada Seismic Belt, *J. Geophys. Res.*, 108(B8), 2394, doi:10.1029/2002JB002257.
- Jennings, C. W. (1994), Fault activity map of California and adjacent areas, *Calif. Geol. Data Map Ser. Map, 6*, scale 1:750,000, Calif. Div. of Mines and Geol., Sacramento.
- Johnson, M. G. (1977), Geology and mineral deposits of Pershing County, Nevada, *Nev. Bur. Mines Geol. Bull.*, 89, 1–115.
- Jones, C. H., J. R. Unruh, and L. J. Sonder (1996), The role of gravitational potential energy in active deformation in the southwestern United States, *Nature*, 381, 37–41.
- Kostrov, V. V. (1974), Seismic moment and energy of earthquakes and seismic flow of rocks, *Izv. Acad. Sci. USSR Phys. Solid Earth, Engl. Transl.*, 1, 23–44.
- Layman, E. B. (1984), A simple Basin and Range fault model for the Beowawe geothermal system, Nevada, *Trans. Geotherm. Resour. Council*, 8, 451–456.
- Lund, W. R. (2004), Utah Quaternary fault parameters working group: Review of Utah paleoseismic-trenching data, final technical report, Grant Award 03HQGR0033, 159 pp., U.S. Geol. Surv., Natl. Earthquake Hazards Reduction Program, Washington, D. C.
- Machette, M. N. (1978), Dating Quaternary faults in the southwestern United States by using buried calcic horizons, *J. Res., U.S. Geol. Surv.*, 6, 369–381.
- Machette, M. N., S. F. Personius, A. R. Nelson, D. P. Schwartz, and W. R. Lund (1991), The Wasatch fault zone, Utah; segmentation and history of Holocene earthquakes, *J. Struct. Geol.*, 13(2), 137–149.
- Machette, M. N., S. F. Personius, and A. R. Nelson (1992), Paleoseismology of the Wasatch fault zone: A summary of recent investigations, interpretations, and conclusions, *U.S. Geol. Surv. Prof. Pap.*, 1500-A-J, A1–A71.
- Machette, M. N., K. M. Haller, K. Okumura, C. A. Ruleman, S. Debray, and S. Mahan (2002), Paleoseismology of the Clan Alpine Fault, west-central Nevada, *Geol. Soc. Am. Abstr. Programs*, 34(4), 3.
- McCalpin, J. (1996), *Paleoseismology*, 588 pp., Springer, New York.
- McCalpin, J., and S. P. Nishenko (1996), Holocene paleoseismicity, temporal clustering, and probabilities of future large ( $M > 7$ ) earthquakes on the Wasatch fault zone, Utah, *J. Geophys. Res.*, 101, 6233–6253.
- Minster, J. B., and T. H. Jordan (1984), Vector constraints on Quaternary deformation of the western United States east and west of the San Andreas Fault, in *Tectonics and Sedimentation Along the California Margin*, edited by J. K. Crouch and S. B. Bachman, pp. 1–16, Pac. Sect., Soc. of Econ., Paleontol. and Mineral., Los Angeles, Calif.
- Oldow, J. S., G. Kohler, and R. A. Donelick (1994), Late Cenozoic extensional transfer in the Walker Lane strike-slip belt, Nevada, *Geology*, 22, 637–640.
- Olig, S. S., A. E. Gorton, B. D. Black, and S. L. Forman (2001), Paleoseismology of the Mercur fault and segmentation of the Oquirrh–East Great Salt Lake fault zone, technical report, grant 98HQGR1036, U.S. Geol. Surv., Reston, Va.
- Owen, L. A., M. C. Sharma, and R. C. Finkel (2001), Natural and human induced landslides in the landscarp evolution of the Garhwal Himalaya, northern India, *Geomorphology*, 40, 21–35.
- Owen, L. A., R. C. Finkel, R. C. Ma, J. Q. Spencer, P. L. Barnard, and M. W. Caffee (2003), Timing and style of Late Quaternary glaciations in NE Tibet, *Geol. Soc. Am. Bull.*, 11, 1356–1364.
- Personius, S. F., R. E. Anderson, K. Okumura, S. Mahan, and D. A. Hancock (2002), Preliminary paleoseismology of the Santa Rosa Range fault zone, Humboldt County, Nevada, *Geol. Soc. Am. Abstr. Programs*, 34(6), 27.
- Ramelli, A. R., J. W. Bell, C. M. dePolo, and J. C. Yount (1999), Large-magnitude, late Holocene earthquakes on the Genoa fault, west-central Nevada and eastern California, *Bull. Seismol. Soc. Am.*, 89, 1458–1472.
- Ramelli, A. R., J. W. Bell, and C. M. dePolo (2004), Peavine Peak: Another piece of the Walker Lane puzzle, in *Basin and Range Province: Seismic Hazards Summit*, pp. 126–127, Nev. Bur. of Mines and Geol., Reno, Nev.
- Reheis, M. (1999), Extent of Pleistocene lakes in the western Great Basin, *U.S. Geol. Surv. Misc. Field Stud. Map, MF-2323*.
- Reheis, M. C., and T. H. Dixon (1996), Kinematics of the Eastern California Shear Zone, evidence for slip transfer from Owens and Saline Valley fault zones to Fish Lake Valley fault zone, *Geology*, 24, 339–342.
- Richards, B. W. (2000), Luminescence dating of Quaternary sediments in the Himalaya and high Asia: A practical guide to its use and limitations for constraining the timing of glaciation, *Quat. Int.*, 65/66, 31–48.
- Roberts, R. J., K. M. Montgomery, and R. E. Lehner (1967), Geology and mineral resources of Eureka County, Nevada, *Nev. Bur. Mines Geol. Bull.*, 64, 1–152.
- Sarna-Wojcicki, A. M., and J. O. Davis (1991), Quaternary tephrachronology, in *Quaternary Nonglacial Geology: Conterminous U. S.*, edited by R. B. Morrison, pp. 93–116, Geol. Soc. of Am., Boulder, Colo.
- Sauber, J. (1994), Geodetic slip rate for the Eastern California Shear Zone and the recurrence time of Mojave Desert earthquakes, *Nature*, 367, 264–266.
- Sauber, J., W. Thatcher, and S. C. Solomon (1986), Geodetic measurements of deformation in the central Mojave Desert, California, *J. Geophys. Res.*, 91, 12,661–12,674.
- Savage, J. C., M. Lisowski, J. L. Svarc, and K. K. Gross (1995), Strain accumulation across the central Nevada seismic zone, *J. Geophys. Res.*, 100, 20,257–20,269.
- Sella, G. F., T. H. Dixon, and A. Mao (2002), REVEL: A model for Recent plate velocities from space geodesy, *J. Geophys. Res.*, 107(B4), 2081, doi:10.1029/2000JB000033.
- Silberling, N. J., and R. E. Wallace (1967), Geologic map of the Imlay quadrangle, Pershing County, Nevada, *U.S. Geol. Surv. Map, GQ-666*, scale 1:62,500.
- Sonder, L. J., and C. H. Jones (1999), Western United States extension: How the west was widened, *Annu. Rev. Earth Planet. Sci.*, 27, 417–462.
- Stewart, J. H., and E. H. McKee (1977), Geology and mineral deposits of Lander County, Nevada, *Nev. Bur. Mines Geol. Bull.*, 88, 1–59.
- Stuiver, M., and H. A. Polach (1977), Discussion: Reporting of  $^{14}\text{C}$  data, *Radiocarbon*, 19, 355–363.
- Stuiver, M., and P. J. Reimer (1993), Extended  $^{14}\text{C}$  database and revised CALIB radiocarbon calibration program, *Radiocarbon*, 35, 215–230.
- Stuiver, M., P. J. Reimer, and T. F. Braziunas (1998), High-precision radiocarbon age calibration for terrestrial and marine samples, *Radiocarbon*, 40, 1127–1151.
- Swan, F. H., III, K. L. Hanson, and M. M. Angell (2004), Paleoseismic investigations of the Stansbury and mid-valley faults, Skull Valley, Utah, in *Proceedings Volume Western States Seismic Policy Council, Basin and Range Province Seismic Hazards Summit II*, edited by W. Lund, 20 pp., Utah Geol. Surv., Salt Lake City.
- Thatcher, W. (2003), GPS constraints on the kinematics of continental deformation, *Int. Geol. Rev.*, 45, 191–212.
- Thatcher, W., G. R. Foulger, J. B. R. J. Svarc, E. Quilty, and G. W. Bawden (1999), Present-day deformation across the Basin and Range province, western United States, *Science*, 283, 1714–1718.
- Tocher, D. (1956), Movement on the Rainbow Mountain fault, *Bull. Seismol. Soc. Am.*, 46, 10–14.
- Wallace, R. E. (1977), Profiles and ages of young fault scarps, north-central Nevada, *Geol. Soc. Am. Bull.*, 88, 1267–1281.
- Wallace, R. E. (1984a), Fault scarps formed during the earthquakes of October 2, 1915, in Pleasant Valley, Nevada, and some tectonic implications, *U.S. Geol. Surv. Prof. Pap.*, 1274-A, A1–A33.

- Wallace, R. E. (1984b), Patterns and timing of late Quaternary faulting in the Great Basin province and relation to some regional tectonic features, *J. Geophys. Res.*, *89*, 5763–5769.
- Wallace, R. E., D. B. Tatlock, N. J. Silberling, and W. P. Irwin (1969), Geologic map of the Unionville quadrangle, Pershing County, Nevada, *U.S. Geol. Surv. Map, GQ-820*, scale 1:62,500.
- Wesnousky, S. G. (2005), Active faulting in the Walker Lane, *Tectonics*, doi:10.1029/2004TC001645, in press.
- Wesnousky, S. G., and C. H. Willoughby (2003), Neotectonic note: The Ruby-East Humboldt Range, northeastern Nevada, *Bull. Seismol. Soc. Am.*, *93*, 1345–1354.
- Wills, C. J., and G. Borchardt (1993), Holocene slip rate and earthquake recurrence on the Honey Lake Fault Zone, northeastern California, *Geology*, *21*, 853–856.
- Zdanowicz, M., A. Zielinski, and M. S. Germani (1999), Mount Mazama eruption: Calendrical age verified and atmospheric impact assessed, *Geology*, *27*, 617–620.
- 
- A. D. Barron, R. W. Briggs, S. Kumar, and S. G. Wesnousky, Center for Neotectonic Studies, University of Nevada, Reno, NV 89557, USA. (steve@seismo.unr.edu)
- S. J. Caskey, Department of Geosciences, San Francisco State University, San Francisco, CA 94132, USA.
- L. Owen, Department of Earth Sciences, University of California, Riverside, CA 92521, USA.

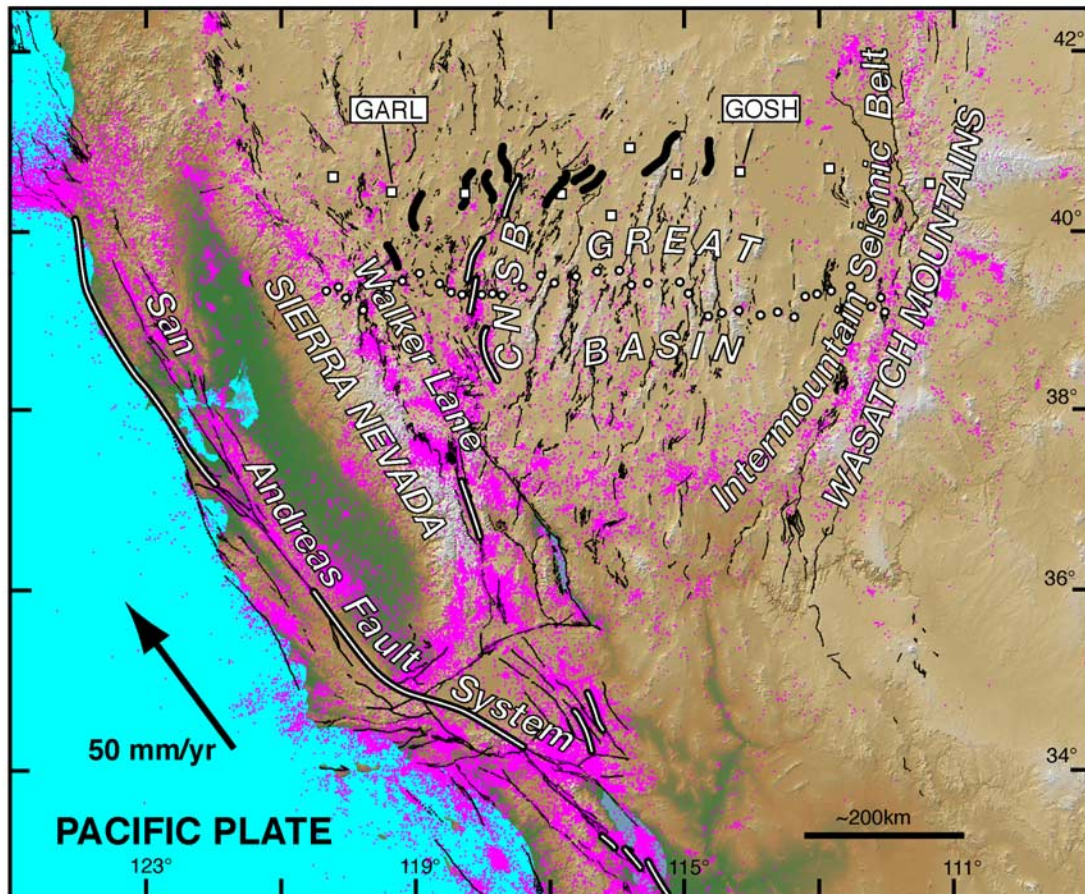


**Figure 1.** Active faults (thin and thick solid lines) and seismicity (dots,  $M > 2$  since 1944) plotted on shaded relief map of Great Basin province and surrounding areas. Thick solid lines denote faults subject to paleoseismological study by authors. Thick open lines are extent of historical earthquake ruptures [Goter *et al.*, 1992]. CNSB is central Nevada seismic belt. Locations of GPS stations surveyed by USGS are shown by open circles south of  $40^{\circ}\text{N}$  [Hammond and Thatcher, 2004; Thatcher, 2003; Thatcher *et al.*, 1999]. Selected GPS station locations of BARGEN array north of  $40^{\circ}\text{N}$  marked by open squares [Bennett *et al.*, 1998, 2003]. Stations GARL and GOSH labeled in reference to discussion in text. Fault map is adapted from parts of Jennings [1994], Dohernwend *et al.* [1996], and the Fault and Fold Database of the U.S. Geological Survey [Haller *et al.*, 2004; <http://qfaults.cr.usgs.gov>]. Seismicity is from the Advanced National Seismic System's composite catalog (<http://quake.geo.berkeley.edu/anss/catalog-search.html>). Plate motion vector is from DeMets and Dixon [1999].